

MID-INFRARED IMAGING OF ORION BN/KL: 11. LUMINOSITY SOURCES,  
EXTINCTION DISTRIBUTION, AND THE NATURE OF IRc2

D. Y. GEZARI<sup>1,4</sup>, D. E. BACKMAN<sup>2,4</sup> and M. W. WERNER<sup>3,4</sup>

<sup>1</sup> NASA/Goddard Space Flight Center, Code 685, Greenbelt, MD 20771

<sup>2</sup> Franklin and Marshall College, Department of Physics and Astronomy,  
P. O. Box 3003, Lancaster, PA 17604

<sup>3</sup> Jet Propulsion Laboratory, California Institute of Technology, MS 233-303,  
4800 Oak Grove Drive, Pasadena, CA 91109

<sup>4</sup> Visiting astronomer at the NASA/Infrared Telescope Facility which is operated by the  
Institute for Astronomy, University of Hawaii.

---

## ABSTRACT

We have obtained array camera images of the Orion BN/KL infrared complex at nine wavelengths between 4.8 and 20  $\mu\text{m}$ . The images are well-sampled and nearly diffraction-limited ( $\sim 1.1$  arcsec FWHM at 12.4  $\mu\text{m}$ ), permitting the luminosities of individual sources and the distributions of color temperature and silicate absorption line strength to be determined with much greater precision than previously possible. The results show temperature peaks near IRc2 and BN, and maximum silicate extinction at IRc2, but otherwise there is little of this small-scale structure seen within the central  $\sim 20$  arcsec. Asymmetrically-distributed circumstellar material and irregular foreground extinction are found to have a strong influence on the observed mid-infrared emission. We find that the luminosity of the infrared source IRc2 itself is  $\sim 1000 L_{\text{sun}}$  (much lower than the generally accepted value) but the significant luminosity source(s) in BN/KL must still be close to IRc2. Our results, considered with recent radio continuum and maser emission observations, suggest that a luminous, early-type star must be embedded near IRc2. The star would be obscured by  $\sim 70$  mag of visual extinction from dust grains both local to IRc2 and distributed along the line-of-sight. The combined heating contributions of this hot star, the stars ionizing two other nearby compact HII regions, and the BN Object can account for the observed  $\sim 10^5 L_{\text{sun}}$  total luminosity of the BN/KL complex.

Key words: Infrared: sources - Infrared: array imaging - ISM: Orion BN/KL  
- ISM: Orion IRc2

## 1. INTRODUCTION

It has not been straightforward to determine which of the compact objects observed in the Becklin-Neugebauer/Kleinmann-Low (BN/KL) infrared complex is the principal source of the  $L \sim 10^5 L_{\text{sun}}$  observed luminosity, which emerges in the infrared as thermal emission from heated, distributed dust grains. Early observations suggested that IRC2 (a modest mid-infrared source near the center of BN/KL with an exceptionally deep  $9.7 \mu\text{m}$  silicate spectral absorption feature) was a unique and very energetic object, and the dominant luminosity source in the infrared complex (Dowries et al. 1981, Wynn-Williams et al. 1984). A single O star (or several early B stars) embedded within the complex could account for the observed luminosity of BN/KL. However, when the last detailed model of the infrared complex was proposed (Wynn-Williams et al. 1984) there was little or no observational evidence for luminous stars in BN/KL (for a comprehensive review of the observational literature see Genzel and Stutzki 1989).

IRC2 initially appeared to coincide with the Orion SiO Maser (Genzel et al. 1979), with the center of a systematic molecular gas outflow traced by  $\text{H}_2\text{O}$  and SiO maser emission (Genzel et al. 1981, Dowries et al. 1982), and with the center of the  $3.8 \mu\text{m}$  polarization vector field (Werner, Dinnerstein and Capps 1982). The polarization data also suggested that there were discrete clumps of scattering material, as well as regions of localized low obscuration, through which heated background material was viewed, which accounted for much of the observed infrared emission structure in BN/KL. The only clearly self-luminous objects identified by these early investigations were the BN Object and IRC2.

Subsequently two compact HII regions (radio continuum point sources) were detected with the Very Large Array (VLA) in the heart of BN/KL at 15 and 22 GHz (Churchwell et al. 1987; Garay, Moran and Reid 1987): radio source “B” (the BN Object) and radio source “T” (coincident with the Orion SiO maser). Then Menten and Reid (1991) discovered a third compact HII region (radio source “L”) in BN/KL. Gezari (1992) registered new mid-infrared images with the VLA data to show that the IRC2 infrared peak was displaced from the SiO maser by  $0.8 \pm 0.2$  arcsec, calling into question the prevailing idea that IRC2 excited the Orion SiO maser and was a unique infrared source in the Galaxy. Gezari (1992) speculated that the dominant luminosity source in Orion BN/KL was not IRC2, but rather a nearby unseen star which is the ionizing source for compact HII region “T”. Menten and Reid (1995) independently concluded that radio source “T” should be a more significant luminosity source in BN/KL than IRC2, and that radio source “L” must also contribute significantly to the observed luminosity of BN/KL.

In this study we have derived more accurate physical properties of the BN/KL infrared complex from a complete set of nearly diffraction-limited array camera images at nine wavelengths between  $4.8$  and  $20 \mu\text{m}$  (listed in Table 1). We have used these results to determine the detailed structure and energy budget of the complex, to re-calculate the luminosity of IRC2, and to update the standard picture of Orion BN/KL.

## 2. INSTRUMENTATION AND OBSERVATIONS

### 2.1. Array Camera System

The 4.8 -12.4  $\mu\text{m}$  images presented here were made with an infrared array camera system (Gezari et al. 1992) developed at NASA/Goddard using a 58 x 62 pixel gallium-doped silicon (Si:Ga) photoconductor array manufactured by Hughes/Santa Barbara Research Center (S BRC). The detector is a hybrid device based on a Hughes CRC-228 switched-FET direct readout (DRO) integrated circuit multiplexer. For the 20.0  $\mu\text{m}$  observations an SBRC 15- 30  $\mu\text{m}$  antimony-doped silicon (Si:Sb) array of the same design was provided by C. McCreight at NASA/Ames Research Center and installed temporarily in the Goddard array camera system. The Si:Ga and Si:Sb arrays use the same multiplexer and are electronically interchangeable with only minor adjustments. Detailed descriptions of the detector architecture, array camera instrument, electronics, and data acquisition system are presented by Gezari et al. (1992).

The optical design of the array camera (Gezari 1989) consists of a single off-axis length parabolic mirror, filter wheels, a cold aperture stop and a system of baffles. The array detector, filters and imaging optics were cooled to 10 K with liquid helium. This simple reflective optical design produces diffraction-limited 5-14  $\mu\text{m}$  images with negligible spatial distortion (less than 1/2 pixel across the array, or less than 1 %). Out-of-field environmental background radiation rejection is better than 99%. An OCLI Corp. 4.4-14.5  $\mu\text{m}$  circular variable filter (CVF) with transmission T - 50%, and a filter wheel containing the broadband ( $\Delta\lambda/\lambda = 0.1$ ) OCLI "Silicate" interference filter set (listed in Table 1), are both mounted close to the cold stop. The spectral bandwidth of the CVF photometer is  $\Delta\lambda/\lambda = 0.04$  at 10  $\mu\text{m}$ , defined by the diameter of the adjacent cold stop. The array camera observing configuration on the IRTF telescope is summarized in Table 1.

The 5-17  $\mu\text{m}$  Si:Ga array was operated at about 1/2 full-well capacity (full well  $\sim 7 \times 10^5$  electrons using a 30 Hz frame rate (30 msec integration time per pixel). The noise equivalent flux density was NEFD =  $0.03 \text{ Jy min}^{-1/2} \text{ pixel}^{-1}$  (10) at 12.4  $\mu\text{m}$  using the broadband ( $\Delta\lambda/\lambda = 0.1$ ) interference filter set. The NEFD expressed as noise equivalent brightness is NEB =  $0.45 \text{ Jy min}^{-1/2} \text{ arcsec}^{-2}$  (1  $\sigma$ ). The point source NEFD was PSNEFD  $\sim 0.5 \text{ Jy min}^{-1/2}$  (1  $\sigma$ ) since the point source flux is spread over 20-30 pixels by diffraction and seeing.

For the 20.0  $\mu\text{m}$  observations the Si:Sb array was installed and operated in a similar manner, but with a 60 Hz frame rate to compensate for the higher thermal background at 20  $\mu\text{m}$ . 18.1 and 20.0  $\mu\text{m}$  interference filters ( $\Delta\lambda/\lambda = 0.1$ ) were used. The detector was background limited, and the observational NEFD at 20  $\mu\text{m}$  was  $0.1 \text{ Jy min}^{-1/2} \text{ pixel}^{-1}$  (1  $\sigma$ ). The noise equivalent brightness at 20  $\mu\text{m}$  was NEB =  $1.5 \text{ Jy min}^{-1/2} \text{ arcsec}^{-2}$  (10).

TABLE 1: ARRAY CAMERA OBSERVING CONFIGURATION  
ON THE IRTF TELESCOPE

---

Pixel size	$0.260 (\pm 0.003)$ arcsec pixel <sup>”</sup>
Array field of view ( $\alpha, \delta$ )	15.0 x 16.1 ( $\pm 0.2$ ) arcsec
Diffraction limit ( $1.22 \lambda/D$ )	0.36 arcsec at 4.8 $\mu\text{m}$ 0.93 arcsec at 12.4 $\mu\text{m}$ 1.60 arcsec at 20.0 $\mu\text{m}$
Chopper frequency	3 Hz
Chopper throw	40 arcsec (north)
Frame rate	30 Hz (60 Hz at 20 $\mu\text{m}$ )
integration time	1 min (1800 frames @ 30 msec)
Input focal ratio	f/35
Final focal ratio at array	f/17.5
Fixed filters	7.8, 8.7, 9.8, 10.3, 11.6, 12.4, 18.1, 20.0 $\mu\text{m}$ ( $\Delta\lambda/\lambda$ -0.1, T - 80%)
Circular Variable Filter	4.4 -14.5 $\mu\text{m}$ ( $\Delta\lambda/\lambda = 0.04$ at 10 $\mu\text{m}$ , T - 50%)

---

## 2.2. Observations

The observations were made at the NASA Infrared Telescope Facility (IRTF) on Mauna Kea. 12.4  $\mu\text{m}$  images were obtained on the nights of 15 March 1988, 11 November 1988, and 23 March 1989; 8.7 and 9.8  $\mu\text{m}$  images were made on the night of 11 November 1988, and a complete set of 7.8- 12.4 and 18.1  $\mu\text{m}$  images was made on the night of 4 December 1990. The 20.0  $\mu\text{m}$  mosaic is made up of 23 overlapping 1 min integrations obtained on the night of 9 November 1989, and the 4.8  $\mu\text{m}$  image was made on the night of 21 March 1991. The observed image profile measured from calibration stars under good atmospheric conditions was typically  $1.1 \pm 0.1$  arcsec FWHM at 12.4  $\mu\text{m}$ . The IRTF chopping secondary mirror was driven at 3 Hz with the reference beam 40 arcsec to the north. Detailed discussions of sky subtraction, flat-fielding, and photometric calibration procedures are presented by Gezari et al. (1992), and Gezari (1995).

## 2.3. Photometric Calibration

Standard star calibration fluxes have not previously been established at all of our filter wavelengths. Flux densities corresponding to 0.0 mag were extrapolated to our filter wavelengths from the mid-infrared absolute flux calibration established by Rieke, Lebofsky and Low (1985), i.e.: 0.0 mag =  $36.0 \pm 1.2$  Jy at 10.6  $\mu\text{m}$  and  $9.4 \pm 0.5$  Jy at 21.0  $\mu\text{m}$ . Photometric calibration of the BN/KL images was made using  $\alpha$  Canis Majoris as the primary infrared standard. The photometric calibration values adopted here for  $\alpha$  CMa were extrapolated from a fit to photometric data for  $\alpha$  CMa between 1.65 and 10  $\mu\text{m}$  given in the list of Bright Infrared Standard Stars compiled at the NASA/Infrared Telescope Facility, and to observations at 18 and 20  $\mu\text{m}$  listed in the Catalog of Infrared Observations (Gezari et al. 1993). The magnitude of  $\alpha$  CMa increases monotonically from -1.38 mag at 4.8  $\mu\text{m}$  to -1.46 mag at 20  $\mu\text{m}$ , with estimated uncertainty of -0.02 mag.

The internal uncertainty of flux measurements within a single image (relative photometry) is estimated to be -2% of the peak at BN, limited by the effectiveness of flat-fielding procedures. The absolute calibration uncertainty is estimated at - 10%, due primarily to the variability of atmospheric transmission during the observations and interpolation of the calibration star flux data to our wavelengths. The uncertainty in the 18.1  $\mu\text{m}$  data is estimated to be  $\pm 2070$  due to a possible near infrared light leak which would effect the calibration of the BN Object only- consequently 18.1  $\mu\text{m}$  brightness listed in Table 2 is determined relative to KL/IRc4 rather than BN. Data reduction and image analysis were done with the MOSAIC software package (Varosi and Gezari 1993) written in the Interactive Data Language (IDL).

## 2.4. Astrometric Calibration

Astrometric error is limited by several factors, including telescope tracking, chopper stability, encoder errors, and mechanical flexure. The plate scale of the 58 x 62 array camera at the Cassegrain focus of the IRTF was measured to be  $0.260 \pm 0.003$  arcsec pixel<sup>-1</sup> in both right ascension and declination, with a corresponding field of view of 15.0 x 16.1 arcsec ( $\alpha, \delta$ ). The relative positions of stellar sources in the image can be determined to an accuracy of better than 0.5 pixel, or  $\pm 0.1$  arcsec, by centroid fitting of Gaussian image profiles. Considering these combined effects, relative source positions in a single array field can be determined with an experimental error of  $\sim 0.012$  arcsec per arcsecond of angular distance

measured, but not less than  $\pm 0.1$  arcsec. Details of the astrometric calibration method are described in detail by Gezari (1992).

Calibration of absolute mid-infrared positions in BN/KL is difficult because there are no nearby stars with well determined positions which are also strong mid-infrared sources. A  $-0.6$  arcsec discrepancy had existed between the published infrared and radio continuum positions for the BN Object, which was marginally within the observational errors. However, Menten and Reid (1991) discovered a third 22 GHz point source (“L”)  $-2$  arcsec south of IRc7 which Gezari (1992) identified with a new  $8.7 \mu\text{m}$  source “n”, permitting unambiguous registration of the infrared and radio images. Gezari (1992) determined that the best infrared position for the point-like core of the BN Object was the position of radio point source “B” (Menten and Reid 1991),  $\alpha = 5^{\text{h}}32^{\text{m}}46.64^{\text{s}} \pm 0.01^{\text{s}}$ ,  $\delta = -5^{\circ}24'16.5'' \pm 0.1''$  (1950), and we adopt this position as the absolute infrared position reference in BN/KL.

### 3. RESULTS

#### 3.1. *The 4.8 - 20.0 $\mu\text{m}$ Image Set*

Figure 1 shows the center of a  $12.4 \mu\text{m}$  mosaic covering a 30 arcsec field-of-view, assembled from 12 overlapping images. Figure 2a shows the large-scale  $20.0 \mu\text{m}$  mosaic image of BN/KL (Gezari et al. 1997) covering a  $50 \times 50$  arcsec field-of-view, assembled from 23 individual overlapping  $15.0 \times 16.1$  arcsec images. Note that significant  $20 \mu\text{m}$  emission extends over most of the field, and real diffraction-limited (1 arcsec) structure is apparent down to the  $1 \text{ Jy arcsec}^{-2}$  brightness level ( $5\sigma$ ). Figure 2b shows enlarged detail in the extended  $20.0 \mu\text{m}$  emission from the eastern region of BK/KL (see Section 3.2). Figures 3(a-i) present the calibrated set of images at our nine wavelengths between 4.8 and 20  $\mu\text{m}$ , and the corresponding contour plots. Figure 4 identifies the prominent sources in the field (superimposed on the  $12.4 \mu\text{m}$  image), and Figure 5 (from Gezari 1992) shows the locations of the Orion SiO maser, the  $\text{H}_2\text{O}$  maser cluster, and the positions of 15/22 GHz radio sources “B”, “I”, and “L” with respect to IRc2, IRc7 and BN.

#### 3.2. *New Mid-Infrared Sources in BN/KL*

A total of nine new compact mid-infrared sources have been identified in the images (Table 2). Two new compact sources (NEW #1 and #2) have been detected at  $12.4 \mu\text{m}$ , about 4 arcsec E of IRc2, and three additional new sources (NEW #3 - #5) also appear in the  $20.0 \mu\text{m}$  extended emission nearby (enlarged in Figure 2b). Several additional discrete clumps are seen east of BN in the  $20.0 \mu\text{m}$  mosaic. A new compact peak is seen most prominently in the  $8.7 \mu\text{m}$  image (Figure 3c), 2 arcsec NW of IRc4, which we call IRc4(N). A new, very compact source is seen about 1 arcsec NW of source IRc6, appearing most prominently in the  $7.8$  and  $8.7 \mu\text{m}$  images, which we call IRc6(NW). Because of the high silicate extinction in the region, these seemingly weaker objects may in fact represent a significant additional source of luminosity in the region (see Figure 2). The  $3.8 \mu\text{m}$  point source “n” (Lonsdale et al. 1982) appears clearly about 2 arcsec S and 1 arcsec E of IRc7 in most of the 4.8-  $12.4 \mu\text{m}$  images (Figure 3), particularly at  $8.7 \mu\text{m}$ . As described in Section 2.3, this new mid-infrared source provided a critical third spatial correlation point for the astrometric calibration of the infrared and radio positional reference systems (Gezari 1992).

TABLE2: ORION BN/KL PHOTOMETRY AND ASTROMETRY

		Source Brightness (Jy arcsec <sup>-2</sup> )*									Relative Position** (arcsec)	
Filter	(pm):	4.8	7.8	8.7	9.8	10.3	11.6	12.4	18.1****	20.0	$\Delta\alpha$	$\Delta\delta$
BN	Object	58	149	125	66	88	119	151	-	186	0.0	0.0
IRc2		2	19		3 1	1	8	35	-	56	+5.5	-6.7
IRc3		1	1	1	1	2	5	14	-	99	-1.7	-8.0
IRc4		1	3	2	2	3	11	32	-	147	+1.4	-11.6
IRc5		1	1	1	1	2	4	11	-	91	-0.5	-15.0
IRC6		2	12	3	1	2	4	11	-	84	+0.4	-4.5
1 Rc7		1	6	3	1	2	10	33	-	99	+2.8	-7.8
NEW MID-INFRARED SOURCES												
IRc4(NW)		1	2	3	1	2	6	18	-	(1 20)	0.0	-10.2
IRc6(NW)		3	2	2	1	2	4	11	-	82	0.0	-3.5
"n"		1	3	2	1	(2)	(4)	(13)	-	(48)	+3.6	-9.8
IRC8			<1	1	1	1	1	4	-	45	+8.1	-12.0
NEW #1		<1	1	1	1	1	1	5	-	42	+8.7	-7.7
NEW #2		0.6	0.8	-		0.9	1.1	5.1	-	29.8	+10.0	-7.9
NEW #3		-						3.5	-	34.3	+14.5	-5.1
NEW #4		-						3.7	-	35.2	+14.2	-6.0
NEW #5		-	0.2	0.8	0.6	1.2	0.8	3.0	-	41.5	+6.0	-14.0

(continued on next page)

(Footnotes for Table 2)

\* Peak source brightness ( $\text{Jy arcsec}^{-2}$ ;  $1 \text{ Jy} = 1.0 \times 10^{-26} \text{ Wm}^{-2} \text{ Hz}^{-1}$ ), uncorrected for and including any underlying extended emission at each source position. Brightness is measured in a  $3 \times 3$  pixel ( $0.78 \times 0.78 \text{ arcsec}$ ) box relative to BN at all wavelengths. Upper limits are in parenthesis, and occur when a compact source is not distinct from the surrounding extended emission. Total flux densities can be calculated from the brightness contours in each individual case.

\*\* Positional offsets from the BN Object ( $\alpha = 5^{\text{h}}32^{\text{m}}46.64^{\text{s}} \pm 0.01'$ ,  $\delta = -5^{\circ}24'16.5'' \pm 0.1''$ , epoch 1950). Error in determining the position of a point source on the array is  $\pm 0.1 \text{ arcsec}$  (about half a pixel); uncertainty of the plate scale is  $\pm 0.003 \text{ arcsec pixel}^{-1}$ . The astrometric accuracy of a relative source position is  $\pm 0.012 \text{ arcsec per arcsecond}$  of angular separation of the source from BN in the image.

\*\*\* Absolute  $18.1 \mu\text{m}$  brightness calibration impossible due to inadequate observational data.

### 3.4. Structure of IRc2 and IRc7

#### 3.4.1. Background

Early observations of IRc2 (e.g. Rieke, Low, and Kleinmann 1973, Wynn-Williams and Becklin 1974, Grasdalen, Gherz, and Hackwell 1981, Lee et al. 1983) showed a bright object which appeared to be quite extended (3 x 5 arcsec) from 2 arcsec resolution aperture photometry. Greatly improved knowledge of the IRc2 source profile and position (showing that it was very compact but not clearly resolving it from IRc7) was obtained from one-dimensional speckle interferometry observations of IRc2 at 4.9  $\mu\text{m}$  (Chelli, Perrier and Lena 1984), and linear scans through IRc2 at 7.8 and 12.5  $\mu\text{m}$  along 45° baselines (Lester et al. 1985). The one-dimensional spatial measurements were by nature ambiguous, and the results could be interpreted variously as emission from a disk, a torus, or from an embedded compact object. Evidence for an expanding, rotating 0.15 arcsec diameter disk structure in SiO maser emission on a spatial scale well below our resolution in the mid-infrared has been presented by Plambeck, Wright and Carlstrom (1990).

#### 3.4.2. The New Array Results for IRc2 and IRc7

in the images presented here, IRc2 and IRc7 are resolved at 12.4  $\mu\text{m}$  as two equally bright point sources. A narrow, partially resolved ridge of emission extends west and slightly south from IRc2 directly toward IRc7. IRc2 and IRc7 are separated by  $2.9 \pm 0.1$  arcsec (a projected distance of about 1500 AU at 450 parsecs). The ridge which connects IRc2 and IRc7 appears to be slightly arc-shaped (see Figure 6g and Figure 9), curving around the position of the SiO maser (15 GHz source “1”). The morphology suggests erosion of the ridge by luminous sources near the SiO maser position. While IRc2 is slightly elongated toward IRc7, and the source pair has a general dumbbell-like appearance, we do not see evidence in the mid-infrared array data to support the idea that these two sources together represent a torus of material seen nearly edge-on (previous speculation summarized by Genzel and Stutzki 1989).

The Orion SiO maser is located  $0.8 \pm 0.1$  arcsec S and  $0.1 \pm 0.1$  arcsec E of the IRc2 peak. Note that several other sources and features are also displaced -1 arcsec SE from the peak of IRc2, including the molecular hot core peak (Masson and Mundy 1988, and references therein), the 450  $\mu\text{m}$  continuum emission peak (Wright et al. 1992), the 3-mm continuum peak (Murata et al. 1992, Wright et al. 1996), and the deepest 9.8  $\mu\text{m}$  silicate line absorption (see Section 4.1). These are all indications that IRc2 is not the simple, monolithic source favored by early models, supported by the observations of Dougados et al., (1993) which show that IRc2 breaks up into several distinct sources at 3.8  $\mu\text{m}$ , suggesting the influence of several embedded stars.

Direct images of IRc2 in the deepest part of the broad silicate absorption feature (at 9.8 and 10.3  $\mu\text{m}$ ~ Figure 6d and 6e) show that the detailed appearance of IRc2 changes dramatically at 9.8  $\mu\text{m}$  as compared with the adjacent continuum. At 9.8  $\mu\text{m}$  IRc2 becomes extended south-eastward toward the SiO maser position. There are also significant differences between the 9.8 and 10.3  $\mu\text{m}$  images themselves, a puzzling effect which can not be easily explained. At 10.3  $\mu\text{m}$  only the narrow ridge is visible, and the southerly extension from the IRc2 peak position toward the SiO maser is absent. These structural differences are real and, despite the weakness of the source in the silicate images, not due to noise or array gain defects.

## 4. DERIVED PHYSICAL PROPERTIES

### 4.1. *Silicate Absorption Line Strength "Image"*

The strength of the 9.8  $\mu\text{m}$  silicate absorption feature over the whole field of view can be calculated for every pixel in the mosaic from the ratio of the observed flux at 9.8  $\mu\text{m}$  to the continuum (interpolated between 7.8 and 12.4  $\mu\text{m}$ ) and displayed as an image (Figure 7). The line strength varies markedly among the IRc sources and is dramatic in the vicinity of IRc2. The 9.8  $\mu\text{m}$  silicate absorption at IRc2 (calculated as the ratio of the 9.8  $\mu\text{m}$  peak brightness in a 3 x 3 pixel aperture to the continuum interpolated between 7.8 and 12.4  $\mu\text{m}$ ) is a factor of 72 (4.6 mag), corresponding to  $A_v = 62 \pm 10$  mag visible extinction (uncertainty due primarily to the extinction law extrapolation). Using the same approach for BN, the 9.8  $\mu\text{m}$  absorption is a factor of 2.3 (0.9 mag), corresponding to  $A_v = 12$  mag extinction in the visible.

It seems likely that most of the absorbing grains toward the heavily obscured IRc2 complex are close to those sources (discussed further in section 5.3) because the image of 9.8  $\mu\text{m}$  silicate strength (Figure 7) shows structure which is roughly correlated with the mid-infrared sources, and the amount of extinction is found to be substantially different from position to position in the field. In the region near IRc3, IRc4 and KI., the absorption strength is uniform within a factor of  $\sim 2$ , indicating less extinction associated with source structure and a relatively uniform temperature distribution (e.g. Figure 8) in this portion of the complex. Useful observations in the 18  $\mu\text{m}$  silicate feature were obtained with the 18.1 and 20.0  $\mu\text{m}$  filters, however, a lack of corresponding continuum data outside the line (at 24  $\mu\text{m}$ , for example) precluded further quantitative analysis here.

### 4.2. *Extinction Correction for IRc2 and BN*

For the purposes of deriving source color temperature, luminosity, etc. the observations were de-reddened using extinction corrections based on our observations of the strength of the broad 9.7  $\mu\text{m}$  silicate feature (the line-to-continuum ratio), extrapolated to longer and shorter wavelengths using the empirical interstellar extinction law of Rieke and Lebofsky (1975). The de-reddened spectra are used to estimate the color temperatures and luminosities of IRc2 and the BN Object.

The model extinction corrections in Table 3 (obtained from the corrected total flux density results) are slightly higher than extinctions that would be calculated from the peak image brightness data (Table 2) based on the 9.8  $\mu\text{m}$  line strengths measured directly from the images (see Section 4.1). Consequently, the luminosities calculated in Section 4.4 represent likely luminosity upper limits for both BN and IRc2.

TABLE 3: DE-REDDENED OBSERVATIONS OF IRc2 AND BN

Source	$\lambda(\mu\text{m})$	Total Flux Density (Jy)		Extinction Correction (magnitudes)
		Observed	Corrected	

IRC2	4.8	10	48	1.7
	7.8	<b>80</b>	220	1.1
	9.8	1	250	6.0
	12.4	140	810	<b>1.9</b>
	20.0	<b>105</b>	550	1.9

---

BN	Object	4,8	225	310	0.34
		7.8	350	430	0.22
		9.8	175	530	1.20
		12.4	525	750	0.39
		20.0	<b>615</b>	850	0.35

---

#### 4.3. Color Temperature “Image”

The color temperature distribution over the whole field-of-view can be obtained with 1arcsec resolution from color ratios using various combinations of the de-reddened 3.8,7.8, 12.4 and 20  $\mu\text{m}$  array data. Figure 8 shows an “image” of the color temperature distribution calculated from the 12/20  $\mu\text{m}$  brightness ratio. The wavelength dependence of emissivity has taken to be  $\epsilon(\lambda) = \text{constant}$  for color temperature calculations because of the small wavelength range and complexity of the silicate spectrum, and it should be noted that a  $\epsilon(\lambda) \propto \lambda^{-1}$  dependence would result in lower physical grain temperatures.

The highest color temperatures calculated from the 12/20  $\mu\text{m}$  image ratio occur at BN ( $T_c = 475\text{K}$ ) and in an extended area around IRC2 and IRC7 (including the new sources east of IRC2 and south of IRC7), toward the molecular “hot core” (Mangum et al. 1993, Wright et al. 1996), and the 450/800  $\mu\text{m}$  emission peak (Wright et al. 1992). The regions of highest dust temperature should indicate the presence of the principal luminosity sources, based on the simple argument that temperature gradients correspond to the direction of energy flow. Although this interpretation can become weakened if localized extinction effects are also considered, it is noteworthy that, even at very high spatial resolution, the warm dust in BN/KL is confined to the vicinity of BN and IRC2, and suggests that the luminosity sources in the complex are localized to those positions.

For IRC2 the de-reddened spectra yield color temperatures of  $T_c = 350\text{K}$  (using the 3.8  $\mu\text{m}$  flux of Dougados et al. 1993 and our 7.8  $\mu\text{m}$  data),  $T_c = 260\text{K}$  using 7.8/12.4  $\mu\text{m}$ , and  $T_c = 500\text{K}$  using 12/20  $\mu\text{m}$  (but only 300 K assuming  $\epsilon(\lambda) \propto \lambda^{-1}$ ). The apparent non-monotonic dependence of color temperature on wavelength is a constraint on possible models for extinction geometries near IRC2. These temperatures are noticeably cooler than the findings of Wynn-Williams et al. (1984), who concluded that IRC2 had the de-reddened spectrum of a  $700 \pm 200\text{K}$  blackbody.

#### 4.4. New Luminosity Estimates for IRc2, BN and the BN/KL Source Complex

We calculated the luminosity for IRc2 by fitting a simple blackbody model spectrum to the de-reddened observations (see Table 3), assuming that the radiation from IRc2 is isotropic and that the silicate feature is not filled in by emission from a foreground source.. A more elaborate model which incorporates varying ratios of silicate and graphite grains in the emitting source and along the line-of-sight produced similar luminosity results. However, a preferred model could not be selected because different Si/C abundance ratios (to which the model luminosity result is quite sensitive) seem fit the limited spectral range data equally well.

We find that the apparent de-reddened luminosity of IRc2 is  $L = 1000 \pm 500 L_{\text{sun}}$  (dramatically lower than previous values as high as  $\sim 10^5 L_{\text{sun}}$ ) with corresponding model source parameters  $T = 350\text{K}$ ,  $A_v = 70$ , and source size  $9 \times 10^{-13}$  Sr. While the derived properties are only a rough estimate, it is clear that the luminosity of IRc2 need not be higher than about  $1000 L_{\text{sun}}$  to account for the observed mid-infrared data. Our result can be reconciled with the higher earlier estimates, as discussed in Section 5.1.

Using the same approach, the luminosity of the BN Object is about  $2000 L_{\text{sun}}$  (comparable to previous determinations) with corresponding model parameters  $T = 550\text{K}$ ,  $A_v = 14$  mag, and source size of  $2 \times 10^{-13}$  Sr. This luminosity is consistent with emission from a substantial circumstellar dust cloud surrounding a main sequence B3 - B4 star.

The bolometric luminosity of the entire Orion BN/KL source complex (central 50 arcsec) can be accurately estimated using our de-reddened mid-infrared array data, far-infrared photometry (Beichman, Dyck and Simon 1978, Thronson et al. 1978), the improved high spatial resolution sub-mm maps of Wright et al. (1992), and the 1-mm data of Elias et al. 1975. The over-all peak of the spectral energy distribution appears to be near 50  $\mu\text{m}$ , so most of the luminosity is in the wavelength decade shortward of that (the 5-20  $\mu\text{m}$  band which we imaged). Since the strong 450-800  $\mu\text{m}$  flux does not extend beyond the field of view imaged in our 20.0  $\mu\text{m}$  mosaic (Figure 2), we assume that essentially all of the luminosity produced by sources in BN/KL is emitted or re-radiated from within the 50 arcsec region considered here. From the mid-infrared, far infrared and sub-mm observations the total estimated flux in a 50 arcsec aperture is  $\sim 1.3 \times 10^{-8} \text{Wm}^{-2}$ , corresponding to a total bolometric luminosity for BN/KL of  $L = 8 \times 10^4 L_{\text{sun}}$  (assuming a distance of 450 pc and a non-favored observer's position).

## 5. DISCUSSION

### 5.1. Reconciling the New IRc2 Luminosity with Previous Results

The luminosity we have calculated for IRc2 ( $\sim 1000 L_{\text{sun}}$ ) from the de-reddened array data is 2-3 orders of magnitude lower than previous estimates. The original idea that IRc2 could be the dominant luminosity source in BN/KL (Dowries et al. 1981, Wynn-Williams et al. 1984) was based on large aperture photometry showing a strong, quite warm, extended (3 x 5 arcsec) mid-infrared source, subject to high extinction. Because IRc2 and IRc7 were not resolved as separate sources, the measured flux of IRc2 was actually the sum of the two, which was further increased by the large extinction correction applied. The  $\sim 10^5 L_{\text{sun}}$  luminosity for IRc2 estimated by Wynn-Williams et al. (1984) resulted from a high estimated

extinction toward IRc2 (8 -11 mag at 3.8  $\mu\text{m}$ ), which depended on the assumption that the highly polarized (40%) 3.8  $\mu\text{m}$  emission from IRc3 is scattered light and on the further assumption that IRc2 (the illuminating source for this scattered light) radiated isotropically. The high extinction estimates lead to large color corrections and an excessively high corrected color temperature ( $T = 700 \pm 200$  K) for IRc2. The results were consistent with a “hot”, luminous IRc2, and led to a corresponding correction of luminosity for IRc2 from  $500 L_{\text{sun}}$  observed up to  $0.5\text{-}2 \times 10^5 L_{\text{sun}}$  (Wynn-Williams et al. 1984) .

Our results can be reconciled with those of Wynn-Williams et al. (1984) by considering several observational differences. Our images resolve IRc2 and IRc7 as separate, compact sources, and thus more accurately characterize IRc2 independent of IRc7. Therefore both our observed flux density and color temperature we determine for IRc2 are considerably lower than previous values which were based on low-resolution aperture photometry. While the extinction to IRc2 calculated by Wynn-Williams et al. (1984) corresponds to -4 mag at 12  $\mu\text{m}$ , our high spatial resolution images in the 9.7  $\mu\text{m}$  silicate feature yield extinction to IRc2 of only -1.9 mag at 12.4  $\mu\text{m}$  (where the spectrum of IRc2 peaks), almost an order of magnitude less attenuation than they adopted and further reducing the upward luminosity correction.

Finally, the 3.8  $\mu\text{m}$  emission from IRc3 could indeed be scattered radiation originating from IRc2 (but from a much lower luminosity IRc2 source than previously estimated) if IRc2 is a dense disk or torus oriented roughly edge-on to us with the warm core of the disk exposed in the general direction of IRc3. The hotter, inner regions could directly illuminate IRc3 but be obscured from us by the plane of the disk, while the IRc2 color temperature we observe would be that of the cooler outer regions of the disk. The warm core could have a temperature of about 1000K and luminosity as low as  $5 \times 10^3 L_{\text{sun}}$  in order to account for all of the observed 3.8  $\mu\text{m}$  IRc3 brightness as scattered light from IRc2.

## 5.2. Luminosity Sources Near IRc2

The arguments we have presented here, while not conclusive, are still quite compelling. They suggest a scenario in which IRc2 is not the dominant luminosity source for the BN/KL complex. If this is indeed the case, then an alternate source of luminosity must be identified. The color temperature peak (Figure 8) and the orientation of the 3.8  $\mu\text{m}$  polarization vectors strongly suggest that the likely candidates for such a luminosity source are the presumed O-B star which ionizes the HII region “I”, as well as the infrared source “n” (radio “L”). But we have observed infrared source “n” at a number of infrared wavelengths (Table 2) and find that - in comparison with BN and IRc2 -it is neither exceptionally bright nor has an unusually deep silicate absorption feature. Thus there is no indication from the present infrared data that “n” itself is a particularly luminous source, although the star ionizing the associated compact HII region (radio source “L”) may be quite luminous.

The ionizing star for compact HII region “I” would have to be B3V type or earlier (Churchwell et al. 1987) corresponding to a luminosity of at least  $3 \times 10^3 L_{\text{sun}}$ . Such a luminous star could be present within BN/KL but obscured by intervening dust, since because the derived visible extinction to the IRc2 complex is  $A_v = 62$  mag (see Sections 3e and 4a). The apparent erosion of the mid-infrared contours on the south side of the IRc2-IRc7 ridge near “I” (Figure 6), seen most clearly in several of the best individual 12.4  $\mu\text{m}$  images before co-adding (Figure 9) also supports the idea that an early-type star is embedded at this position.

### 5.3. Implications of the Dust Extinction Distribution

It has been clear from the preceding discussion that extinction both from patchy line-of-sight clouds and circumstellar dust complicate our view of the luminosity sources in BN/KL. Submillimeter and microwave observations (e.g. Wright et al. 1992- Mangum et al. 1993- Wright, Plambeck and Wilner 1996) have identified very dense clouds of dust and gas in the region. The observed anti- correlation of molecular emission and infrared sources demonstrates the role that extinction by cool dust in the foreground molecular clouds plays in the observed morphology of the infrared continuum emission.

Wright, Plambeck and Wilner (1996) made a comprehensive aperture synthesis study which included a 3.5-mm continuum image showing a cool, dense,  $2 \times 3$  arcsec dust condensation centered about 0.5 arcsec E of radio source "I". This dense cloud could easily obscure a hot star such as the ionizing star for radio "I". For example, only  $A_v = 20$  would be required to make a  $m_v = 1$  mag star at "I" undetectable at visible wavelengths. In the mid-infrared the star could only be detected if it was surrounded by a dense circumstellar dust shell. However, no infrared counterpart has been detected, even at wavelengths as long as 20  $\mu\text{m}$ . But given the small scale of the HII region and the fact that the SiO masers are located within -0.1 arcsec of the radio continuum peak, one might expect that this source should be embedded in a cocoon of warm dust. What properties would the dust cloud require to obscure such a warm dust cocoon?

For a luminosity  $L = 10^5 L_{\text{sun}}$  and a size of -0.1 arcsec (45 au. at the distance of the Orion Nebula) this dust cocoon would have  $T = 1000\text{K}$ . At 20  $\mu\text{m}$ , the longest and most penetrating wavelength we have used, the flux from such a cocoon would be  $\sim 4000 \text{ Jy}$  in the absence of foreground extinction. However, the present mid- infrared array data sets a limit of  $\sim 60 \text{ Jy}$  on the observed 20  $\mu\text{m}$  flux from the position of source "I". Therefore, as much as -5 mag of line-of-sight extinction at 20  $\mu\text{m}$  would be required to reduce the flux from the cocoon around source "I" to this level. This is consistent with the observations of Wright, Plambeck and Wilner (1996) showing source "I" at the half-power contour of a dense clump of dust which has an average optical depth of  $\tau = 0.05$  at 3.5- $\mu\text{m}$ , and thus could have  $\tau > 5$  at 20  $\mu\text{m}$ . Note that IRC2 itself is further from the center of this dust condensation than "I" is and would suffer considerably less extinction, although perhaps enough to account for its strong silicate feature.

If a hot star at radio source "I" was a dominant luminosity source in the BN/KL complex, then it presumably could also be the illuminating source for the highly polarized scattered light seen from IRC3 and IRC4. This radiation would be emitted perpendicular to the line-of-sight and need not be influenced by the extinction discussed above. In this scenario, IRC2 itself could be a scattering clump, heated and illuminated externally by source "I". The 3.8  $\mu\text{m}$  radiation from IRC2 should then be highly polarized, with electric vector oriented perpendicular to the line of sight to source "I". The orientation of the electric vectors of the 3.8  $\mu\text{m}$  scattered light seen by Werner et al. (1983) was not well-enough determined because of beam dilution to distinguish IRC2 from other illuminating sources. While the higher angular resolution polarimetry observations by Minchin et al. (1991), Dougados et al. 1993 and Aitken et al. (1996) do show some suggestion of changes in polarization angle with position expected if source "I" were, in fact, the dominant underlying 3.8  $\mu\text{m}$  source, much higher (-0.1 arcsec) spatial resolution near infrared polarimetry would be needed to clarify the roles of IRC2 and source "I".

#### 5.4. Other Energetic Sources in BN/KL

Although the preceding discussion has focused on identifying a single primary luminosity source for the BN/KL region, we have seen that it is clearly possible that several sources contribute substantially to the total luminosity. The source of the energetic molecular outflow in BN/KL can now be reconsidered because the improved spatial resolution of the more recent infrared and radio observations has made small positional displacements between various emission features significant. For example, the center of expansion of the low-velocity maser outflow (Genzel et al. 1981) is -5 arcsec from IRC2, a significant distance on the scale of our resolution and hardly a compelling reason to attribute an unusual role to IRC2. However, the compact radio source “L” (infrared source “n”) does fall within the  $\pm 0.1s \times \pm 2''$  error box for the center of expansion, and represents a more likely candidate for the source of the outflow.

What appears to be an extraordinary explosive event in Orion was imaged in  $1.64 \mu\text{m}[\text{FeII}]$  and  $2.12 \mu\text{m}$   $\text{H}_2$  line emission by Allen and Burton (1993), which has generally been interpreted as a bipolar protostellar outflow. An alternate interpretation, that the streamers are shock-illuminated remnant stellar material from a supernova which occurred only 102 years ago, but which could have easily been obscured by dense dust clouds, was offered by Kundt and Yar (1995). Overlaying our  $12.4 \mu\text{m}$  wide-field mosaic image of BN/KL and Ney Allen Nebula on the composite  $[\text{FeII}]/\text{H}_2$  image suggests that the site of this energetic event was in the northern regions of BN/KL. This suggests the presence of another (unseen) energetic source associated with BN/KL, further arguing against the simple view of a single dominant luminosity source in the region.

### 6. CONCLUSIONS

The Wynn-Williams et al. (1984) model for BN/KL, with IRC2 as the dominant source of luminosity, is generally consistent with the present results regarding the basic structure of the complex. But the new high resolution mid-infrared images have led us to consider alternative luminosity mechanisms. None of our results suggest that IRC2 itself is an unusual source in the BN/KL complex. The new picture which emerges has the critical difference that the mid-infrared source IRC2 is not an object of high intrinsic luminosity. Luminous stars must be associated with the compact HII regions “I” and “L”. The localized extinction due to the dust cloud identified by Wright et al (1996) could be great enough to conceal a luminous object from view at  $I < 20 \mu\text{m}$ . The line-of-sight to IRC2 passes through part of this condensation, which would account for the extremely deep silicate absorption observed at IRC2.

We conclude that IRC2 is a dense dust cloud, similar to IRC3 and IRC4, heated primarily by a heavily obscured O-B star (at the position of the compact HII region “I” and the Orion SiO maser). While the present data support idea that objects like IRC3 and IRC4 do not contain substantial embedded luminosity sources, the contributions of the other compact sources (particularly the BN object) are significant and must also be considered. The combined contributions of the ionizing stars, stars imbedded in the compact IRC sources and the BN Object can account for the observed infrared luminosity of the BN/KL complex.

## ACKNOWLEDGEMENTS

We thank Frank Varosi at NASA/GSFC for his continuing valuable contributions to the array camera program, and Craig McCreight and Mark McKelvey at NASA/Ames for their important contributions to the success of the 20  $\mu\text{m}$  observations. Mary Hewitt of Hughes/Santa Barbara Research Center, and Walter Folz of NASA/GSFC, played key roles in the success of the infrared array camera instrument. We thank Mike Hauser and Chuck Bennett for their encouraging support of the Array Camera program at Goddard. Suvi Gezari contributed to the data analysis effort. Parts of this research were carried out at the Jet Propulsion Laboratory, California Institute of Technology, under contract to the National Aeronautics and Space Administration. The poi used to bless the array camera at the summit of Mauna Kea was provided by Jimmy's Drive-Inn of Hi lo, Hawaii. This work was supported by NASA/OSSA RTOP 188-44-23-08.

## BIBLIOGRAPHY

- Aitken, D. A., Smith, C. H., Moore, T. J. T., Roche, P. F., Fujiyoshi, T., and Wright, C. M. 1996, M. N. R. A. S., (in press).
- Allen, D. A. and Burton, M. G. 1993, Nature, 363,54. Beichman, C. A., Dyck, H. M. and Simon, T. 1978, Astr. Ap., 62,261.
- Chelli, A., Perrier, C., Lena, P. 1984, Ap. J., 280, 163.
- Churchwell, E., Felli, M., Woods, D. O. S., Massi, M. 1987, Ap. J., 321,516.
- Dougados, C., Lena, P., Ridgway, S. T., Christou, J. C., Probst, R. G. 1993, Ap. J., 406, 112.
- Dowries, D., Genzel, R., Becklin, E. E., and Wynn-Williams, C. G. 1981, Ap. J., 244, 869.
- Downes, D., Genzel, R., Hjalmanson, A., Nyman, L. A., and Ronnang, B. 1982, Ap. J.(Letters), 252, L29.
- Elias, J. H., Ennis, D. J., Gezari, D. Y., Hauser, M. G., Houck, J. R., Lo, K. Y., Mathews, K., Nadeau, D., Neugebauer, G., Werner, M. W. and Westbrook, W. E. 1978, Ap. J., 220,25.
- Fischer, J. 1991, private communication.
- Garay, G., Moran, J. M., and Reid, M. J. 1987, Ap. J., 314,535.
- Genzel, R., Moran, J. M., Lane, A. P., Predmore, C. R., Ho, P. T. P., Hansen, S. S., and Reid, M. J. 1979, Ap. J. (Letters), 231, L73.
- Genzel, R., Reid, M. J., Moran, J. M., and Dowries, D. 1981, Ap. J., 244,844.
- Genzel, R. and Stutzki, J. 1989, Ann. Rev. Astron. Astrophys., 27,41 (see pages 62 and 76 for discussion of IRc2 images).
- Gezari, D. Y. 1992, Ap. J. (Letters), 396, L43.
- Gezari, D. Y. 1995, Proc. I. A. U. Symp. #167: "New Directions in Array Technology and Applications", ed. C. Davis-Phillip, Kluwer Acad. Pub., Dordrecht, (in press).
- Gezari, D. Y., Backman, D. E., Werner, M. W., McKelvey, M. and McCreight, C. 1997, (in preparation for P. A. S. P.).
- Gezari, D. Y., Folz, W., Woods, L., and Varosi, F. 1992, P. A. S. P., 104, 191.
- Gezari, D. Y., Schmitz, M., Pitts, P. and Mead, J. M. 1993, Catalog of Infrared Observations (3rd Edition), NASA RP#1 294.
- Grasdalen, G. L., Gherz R. D., and Hackwell, J. A. 1981, Proc.I.A.U. Symposium #96: "Infrared Astronomy," D. Reidel Pub. Co. (Dordrecht, Holland), 179.

Kundt, W. and Yar, A. 1995, *Ap. and Sp. Sci.*, (submitted).

Lee, T. J., Beattie, D. H., Geballe, T. R., and Pickup, D. A. 1983, *Astr. Ap.*, 127,417.

Lester, D. F., Becklin, E. E., Genzel, R. and Wynn-Williams, C. G. 1985, *A. J.*, 90,2331.

Lonsdale C. J., Becklin E. E., Lee T. J., and Stewart, J. M. 1982, *Astron. J.*, 87, 1819.

Masson and Mundy 1988 Mangum, J. G., Wooten, A. and Plambeck, R. L. 1993, *Ap. J.*, 409,282.

Menten, K. M. and Reid, M. J. (1991), *B. A. A. S.*, 22, No. 4, 1269 (abstract).

Menten, K. M. and Reid, M. J. (1995), *Ap. J. (Letters)*, in press.

Minchin, N. R., Hough, J. H., McCall, A., Burton, M. G., McCaughrean, M. J., Aspin, C., Bailey, J. A., Axon, D. J., and Sate, S. 1991, *M. N. R. A. S.*, 248,715.

Murata, Y., Kawabe, R., Ishiguro, M., Morita, K.-I., Hasegawa, T., and Hayashi, M. 1992, *P. A. S. J.*, 44,381.

Ney, E. P. and Allen, D. A. 1969, *Ap. J. (Letters)*, 155, L193.

Plambeck, R. L., Wright, M. C. H., and Carlstrom, J. E., 1990, *Ap. J.* 348, L65.

Rieke, G. H., Low, F. J., and Kleinmann, D. 1973, *Ap. J. (Letters)*, 186, L7.

Rieke and Lebofsky 1985, *Ap. J.*, 288,618. Rieke, G. H. , Lebofsky, M. J., and Low, F. J. 1985, *A. J.*, 90,900.

Thronson, H. A., Harper, D. A., Keene, J., Lowenstein, R. F., Moseley, S. H. and Telesco, C. M. 1978, *A. J.*, 83,492.

Varosi, F. and Gezari, D. Y. 1993, "Astronomical Data Analysis Software and Systems 11", *P. A. S. P. Conf. Series*, 52, 393.

Werner, M. W., Dinerstein, H. L., and Capps, R. W. 1983, *Ap. J. Letters*, 265, L13.

Weintraub, D. A., Kastner, J. H., and Lowrance P. 1994, "Clouds, Cores and Low Mass Stars," *ASP Conf. Series*, 86,266.

Wright, M. C. H., Plambeck, R. L., and Wilner, D. J. 1996, *Ap. J.*, (in press).

Wright, M., Sandell, G., Wilner, D. J., and Plambeck, R. 1992, *Ap. J.*, 393,225.

Wynn-Williams, C. G., and Becklin, E. E. 1974, *P. A. S. P.*, 86,5.

Wynn-Williams, C. G., Genzel, R., Becklin, E. E., and Downes, D. 1984, *Ap. J.*, 281, 172.

size is 0.26 arcsec and the images are nearly diffraction limited ( $\lambda/D = 0.4$  arcsec at 5  $\mu\text{m}$ , 0.8 arcsec at 10  $\mu\text{m}$ , and 1.6 arcsec at 20  $\mu\text{m}$ ).

*Figure 7:* Silicate absorption strength, calculated from the 9.8  $\mu\text{m}$  line-to-continuum ratio. The strongest attenuation occurs at IRc2 (a factor of 72 relative to the adjacent observed continuum) and is generally correlated with the source structure, suggesting that the **extincting** grains are local to the individual sources. Crosses (+) mark the positions of the sources from Figure 3, and the asterisk (\*) is the position of the SiO maser and radio source “I”.

*Figure 8:* Color temperature distribution in BN/KL, as depicted by the de-reddened 20/12  $\mu\text{m}$  brightness ratio (lighter regions are hotter). The highest color temperatures occur at BN and in a second, extended area which includes IRc2/IRc7, the molecular “hot core” (Mangum et al. (1993) and sub-mm emission peak (Wright et al. 1992). The de-reddened 12/20  $\mu\text{m}$  color temperature near IRc2 is  $T_c = 320$  K assuming  $\epsilon(\lambda) \propto \lambda^{-1}$  (or 550 K with  $\epsilon = \text{const.}$ ).

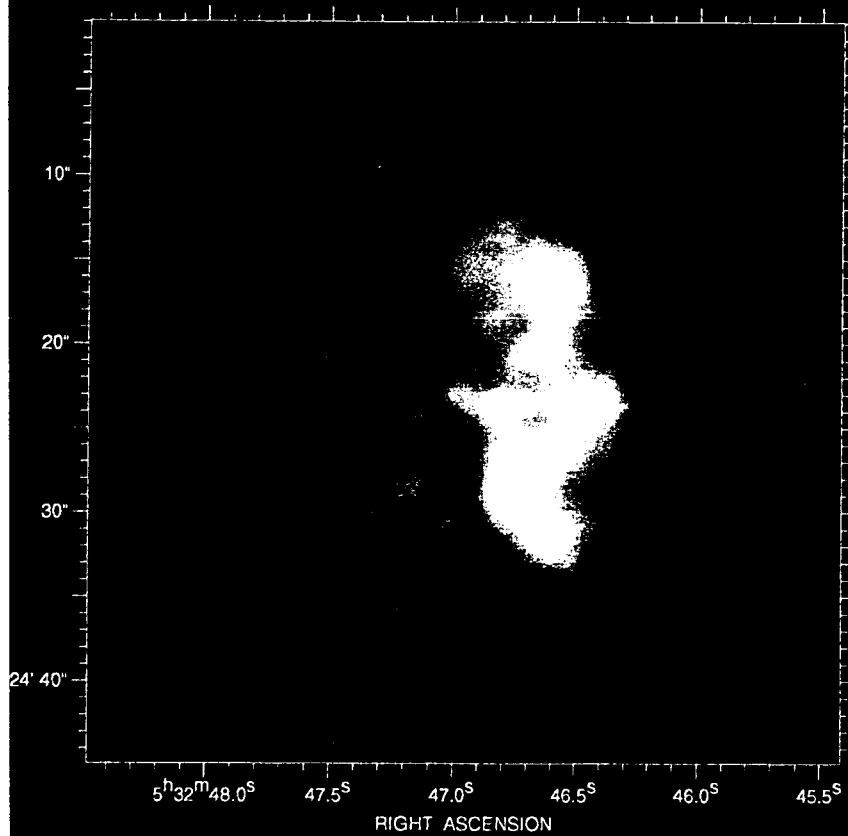
*Figure 9:* Four individual short (3 second) exposures of IRc2 and IRc7 at 8.7  $\mu\text{m}$  showing small-scale structure which is not evident in long integrations because some smoothing occurs when longer (1 minute) integrations are made, and when individual exposures are aligned and co-added to obtain the final integrations (e.g. Figures 3 and 6).

*Figure 10:* 12.4  $\mu\text{m}$  continuum contours of BN/KL and the Ney-Allen Nebula superimposed over a portion of the composite image of the Orion Nebula imaged in 1.64  $\mu\text{m}$  [FeII] and 2.12  $\mu\text{m}$   $\text{H}_2$  line emission (Burton and Allen 1993). The red streamers (upper right) are purported to be the remnants of an extraordinary explosive event which this overlay suggests apparently originated in the northern regions of BN/KL. **The Trapezium stars (at lower left in contour map) are marked with (+) and the extended 12.4  $\mu\text{m}$  emission near the star  $\theta^1\text{D Ori}$  (left-most of the four) is the Ney-Allen Nebula.**



Orion-folder/BN+KL-20CAL.mosaic scratch/contour10-cb.ps  
Scaling: Linear( min= -22. max= 1.3E+02 ) Filter: smooth(3)

Orion BN/KL - 20 um

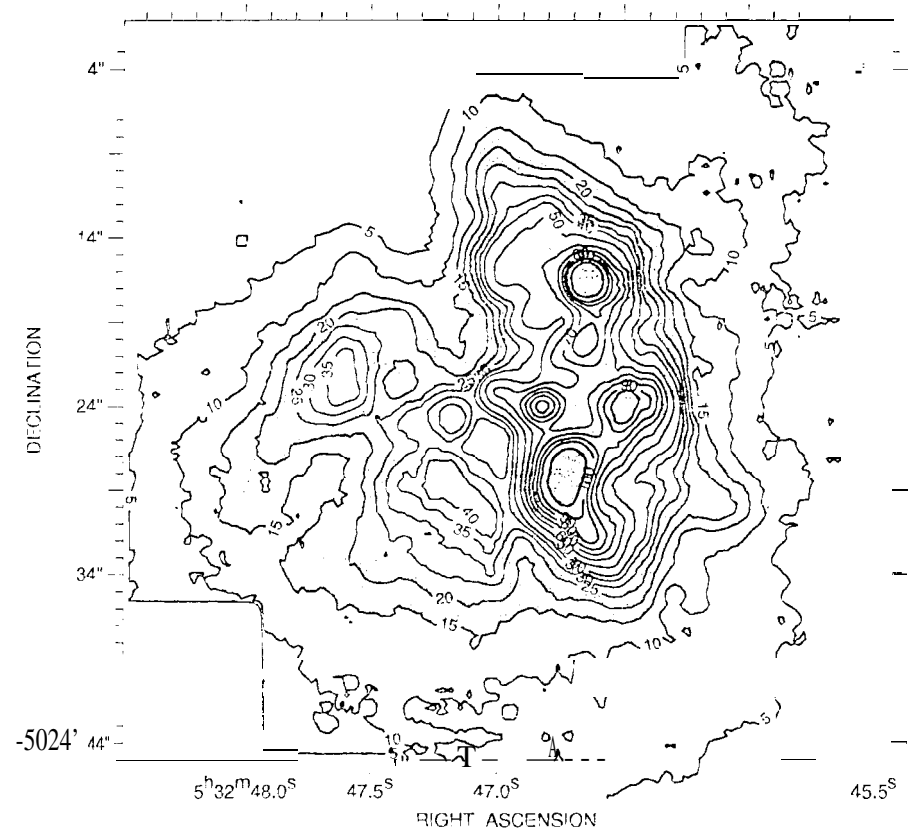


IRTF - Gezari, Backman, Werner, McCreight, McKelvey

NASA/GSFC 6/03/97 D. Gezari

Orion-folder/BN+KL-20CAL.mosaic scratch/contour15-a.ps  
Contours(Linear): min=5.0 inc=5.0 max=1.3E+02 Filter: smooth(3)

Orion BN/KL - 20 um



IRTF - Gezari, Backman, Werner, McCreight, McKelvey

NASA/GSFC 6/03/97 D. Gezari

Fig. 2

Orion BN/KL -20.0 urn

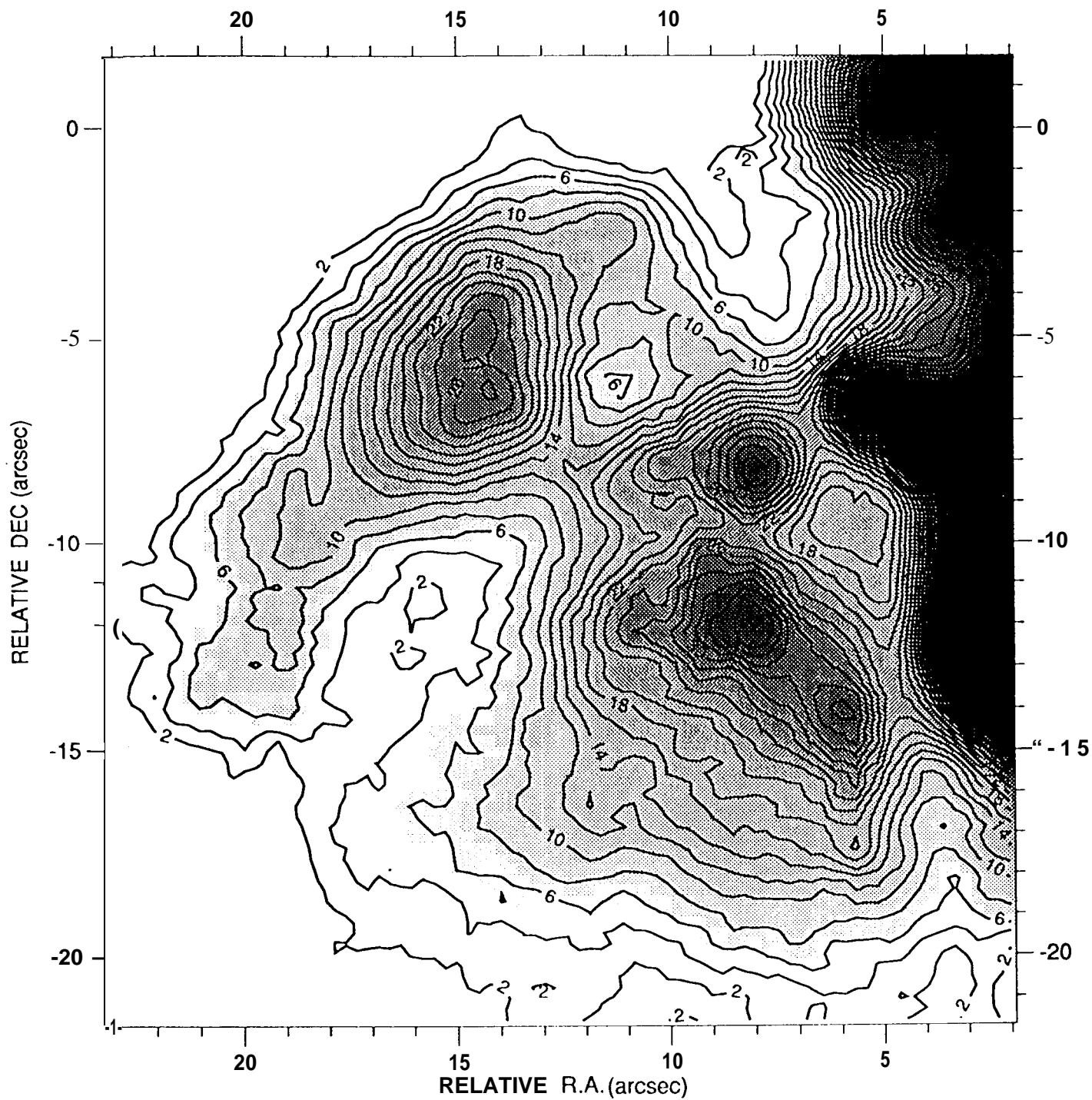


Fig. 2b

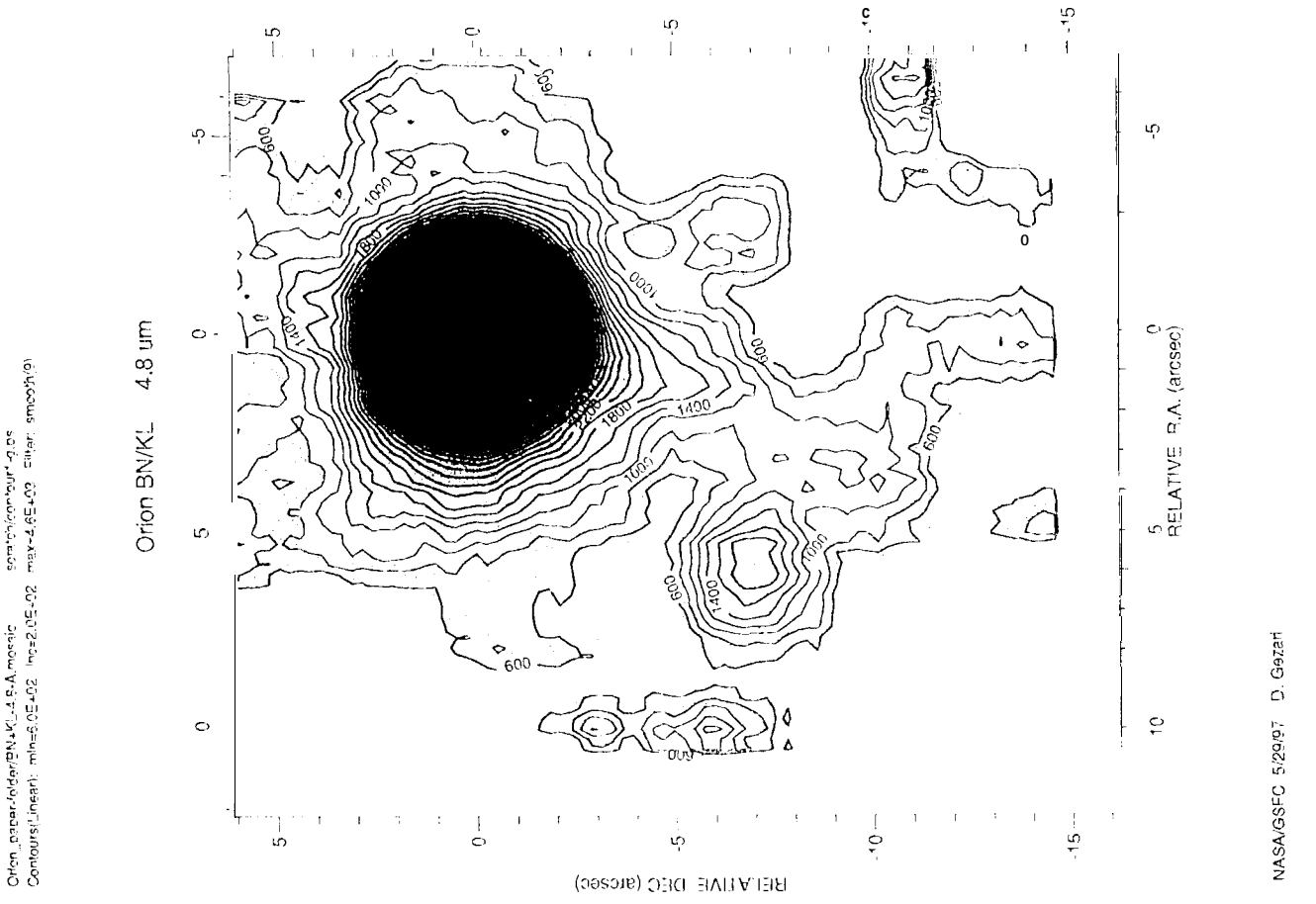
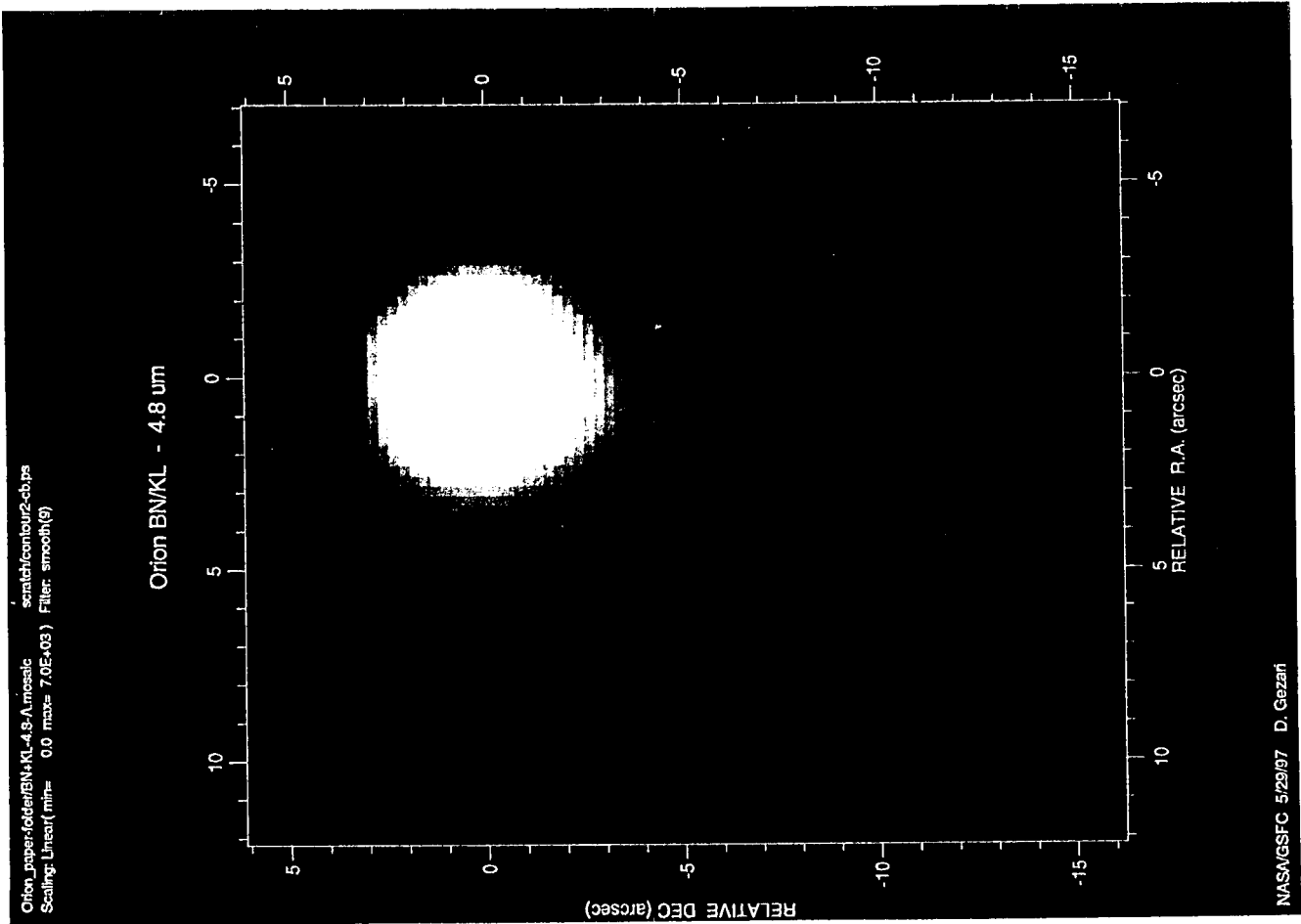
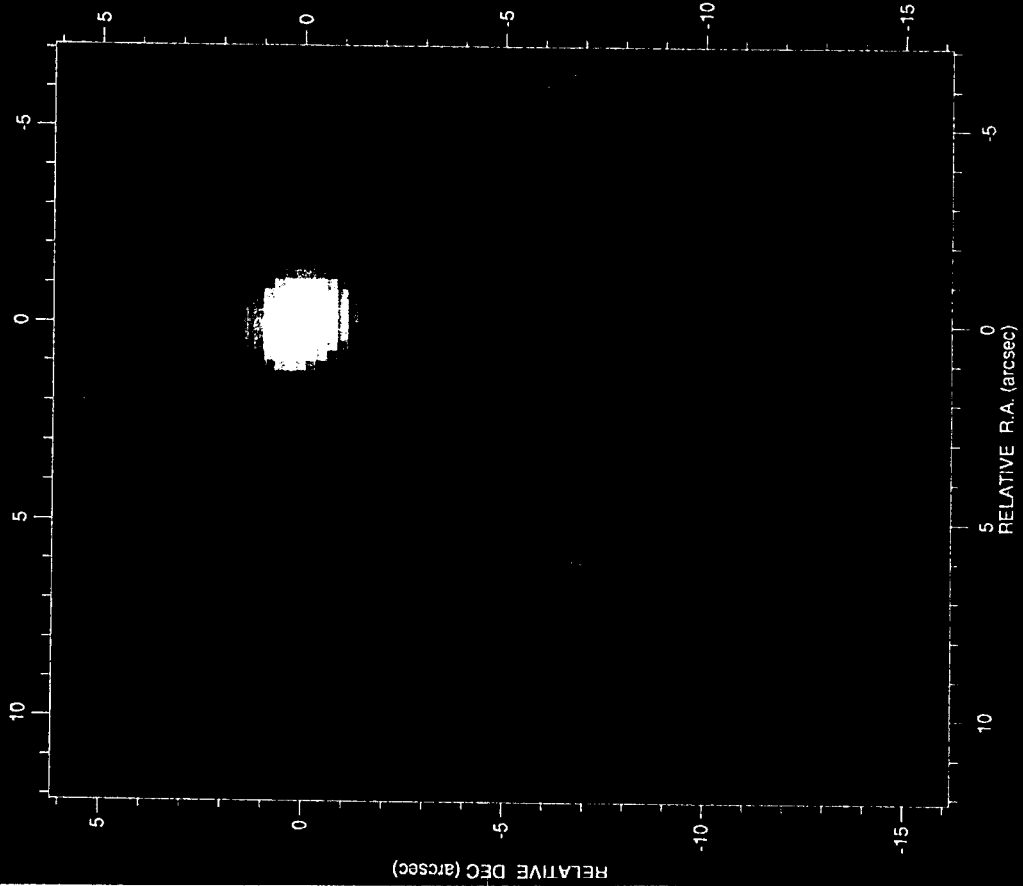


Fig 3a

Orion\_paper\old\er\BN\KL-7.8-A\mosaic  
Scaling: Linear(mih=-1.0E+04 max= 3.0E+05) Filter: smooth(t)

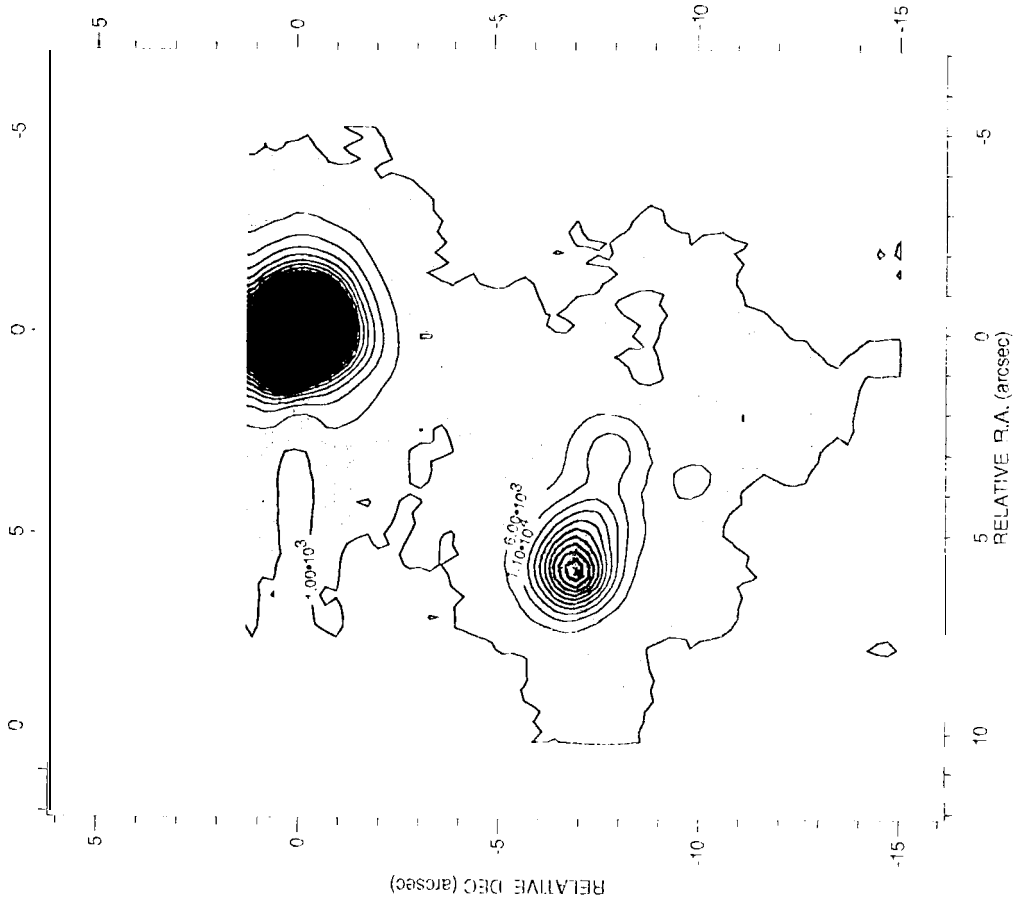
Orion BN/KL - 7.8  $\mu$ m



NASA/GSFC 5/29/97 D. Gezari

Orion\_paper\old\er\BN\KL-7.8-A\mosaic  
scratch\contour20-d.ms  
Contours(Linear: mih=1.0E+03 max=1.5E+05 Filter: smooth(t)

Orion BN/KL - 7.8  $\mu$ m

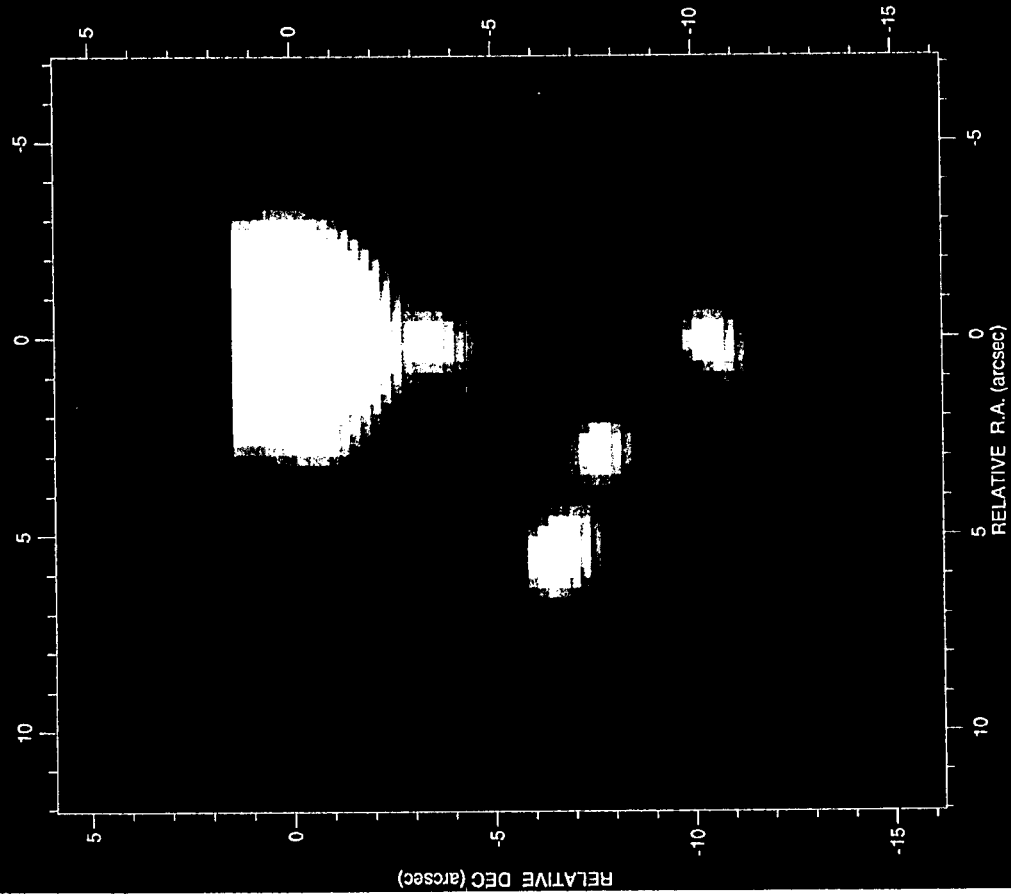


NASA/GSFC 5/29/97 D. Gezari

Fig 3b

Orion\_upperfolder/BN+KL-8.7-A.mosaic  
Scaling: Linear( min= 0.0 max= 1.0E+04) Filter: smooth(5)

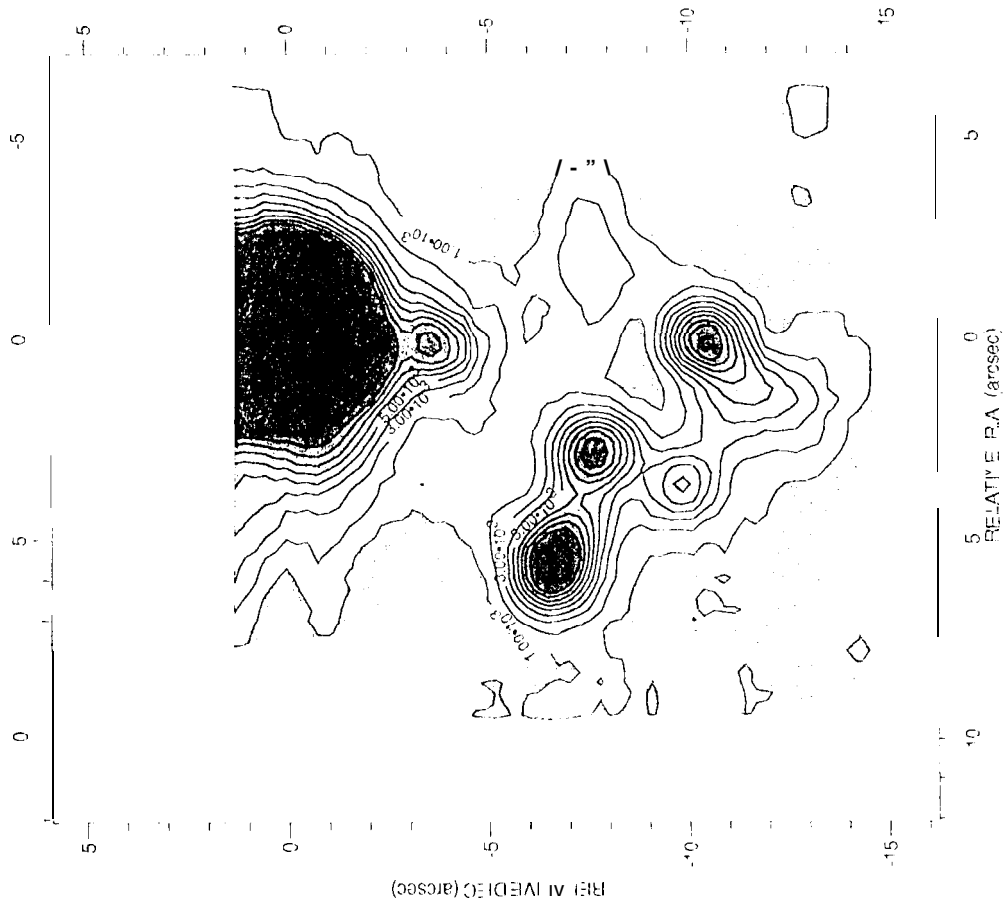
Orion BN/KL - 8.7  $\mu$ m



IRTF 21 MAR 1991  
NASA/GSFC 5/20/97 D. Gezari

Orion\_upperfolder/BN+KL-8.7-A.mosaic  
Contour: Linear( min= 1.0E+03 max= 1.0E+08) Filter: smooth(5)

Orion BN/KL 8.7  $\mu$ m

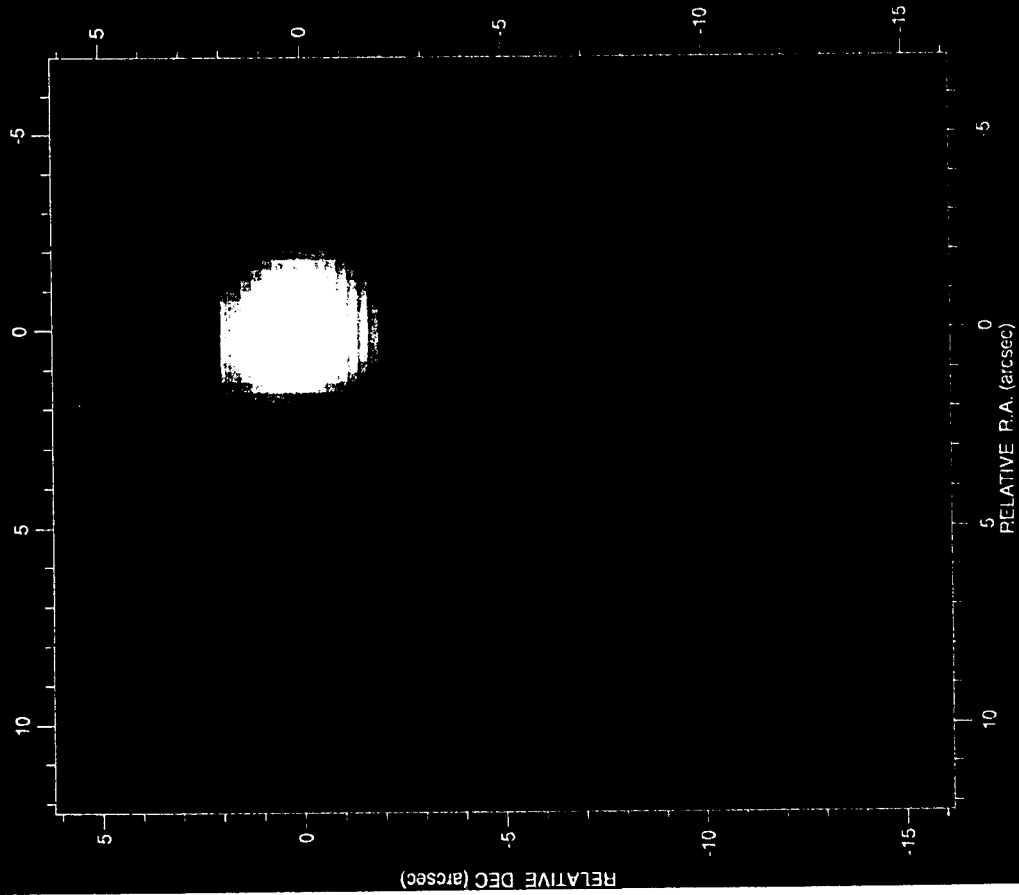


IRTF 21 MAR 1991  
NASA/GSFC 5/20/97 D. Gezari

Fig. 3c

Client\_folder\older\BN\_KL-9.8\_A\_mosaic  
Scaling: Log10 (min= 1.5 max= 4.8) Filter: smooth(S)

BN/KL - 9.8  $\mu$ m



NASA/GSFC 5/29/97 D. Gezari

src\h\con\our2-9.ps  
5 Filter: smooth(S)

BN/KL - 9.8  $\mu$ m

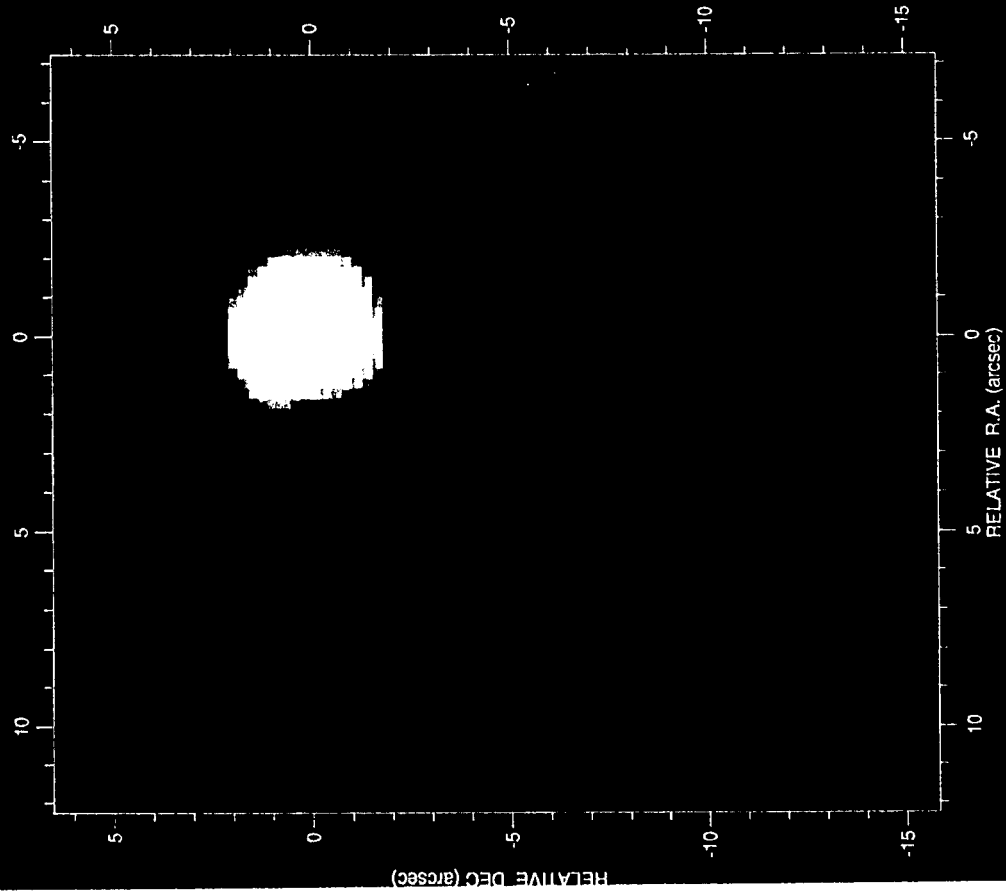


NASA/GSFC 5/29/97 D. Gezari

Fig. 3d

Orion\_bptor-folder/BN/KL-10.3um\_mosaic  
Scaling: Linear( min= 0.0 max= 1.0E+05) Filler: smooth(3)

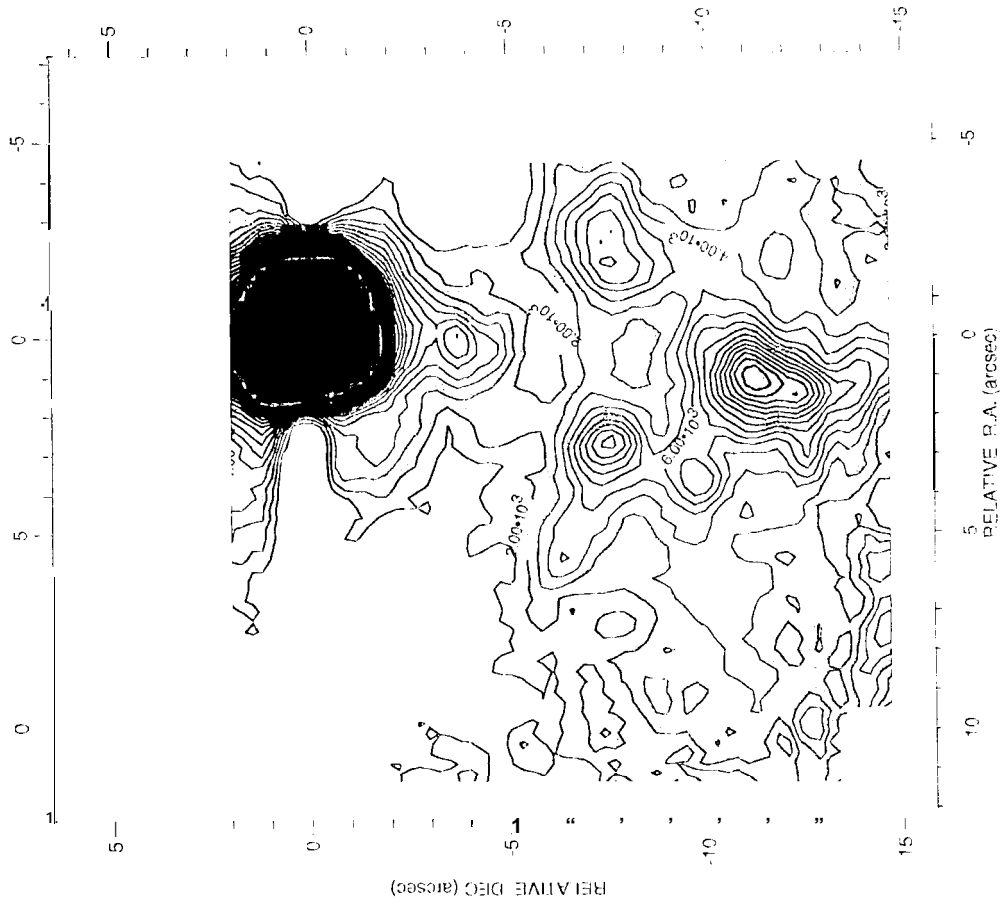
Orion BN/KL - 10.3 um



NASA/GSFC 5/29/07 D. Gezari

Orion\_bptor-folder/BN/KL-10.3um\_mosaic  
Contour: Linear( min=0.0 max=1.0E+03) Filler: smooth(3)

Orion BN/KL - 10.3 um

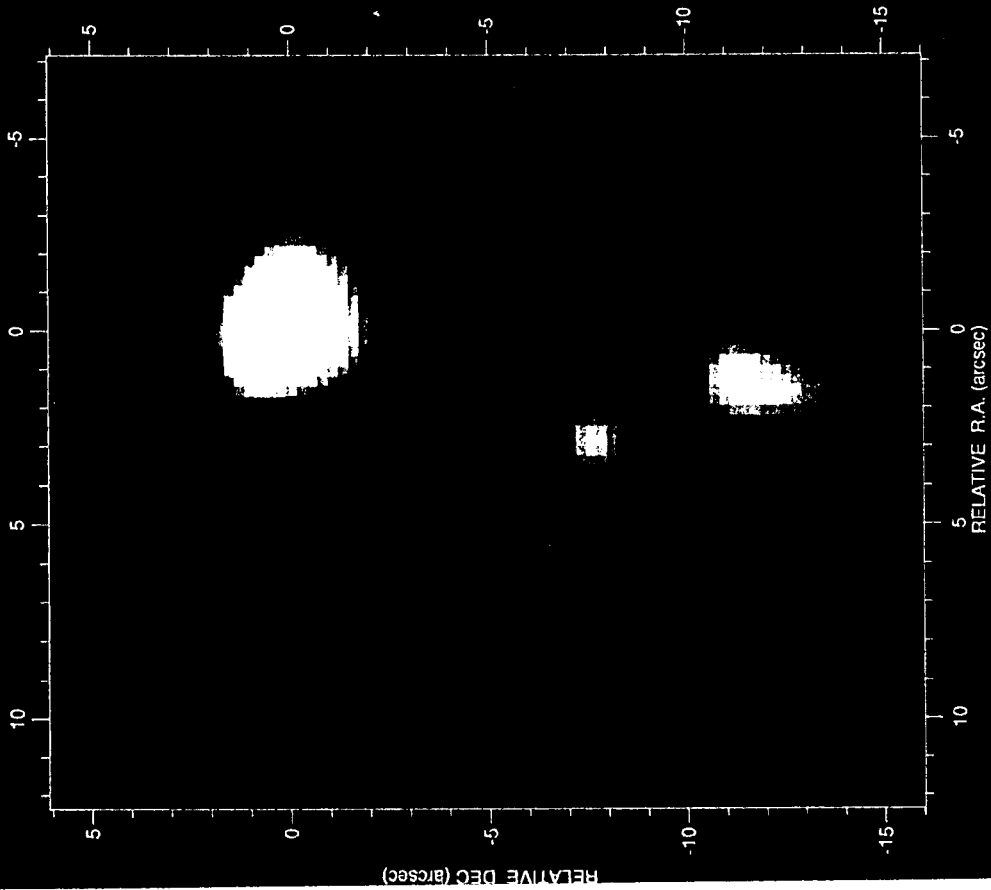


NASA/GSFC 5/29/97 D. Gezari

Fig. 3e

Orion\_paper\folder\BN+KL-11.6-A.mosaic  
Scaling: Linear (min=-1.0E+03 max= 1.0E+05) Filter: smooth(3)

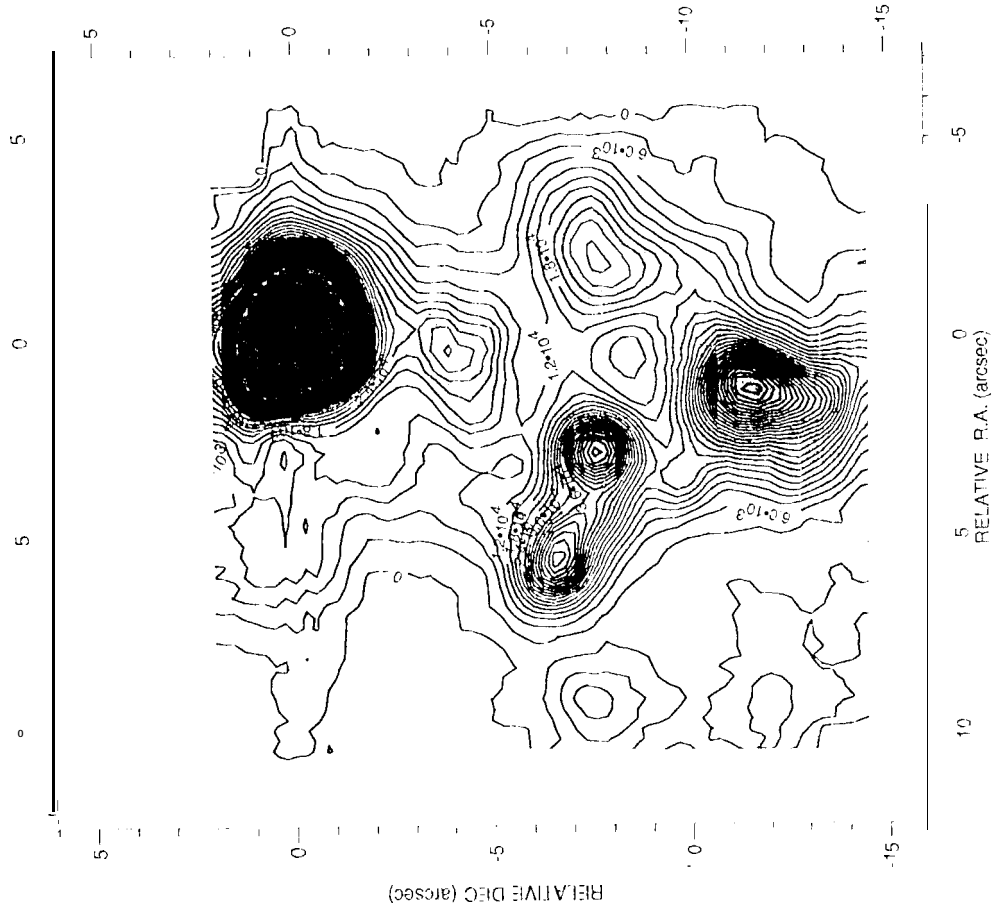
Orion BN/KL - 11.6  $\mu$ m



NASA/GSFC 5/29/97 D. Gezari

Orion\_paper\folder\BN+KL-11.6-A.mosaic  
Contours/Linear: min=0.0 linc=3.0E+03 max=9.7E+04 Filter: smooth(3)

Orion BN/KL 11.6  $\mu$ m

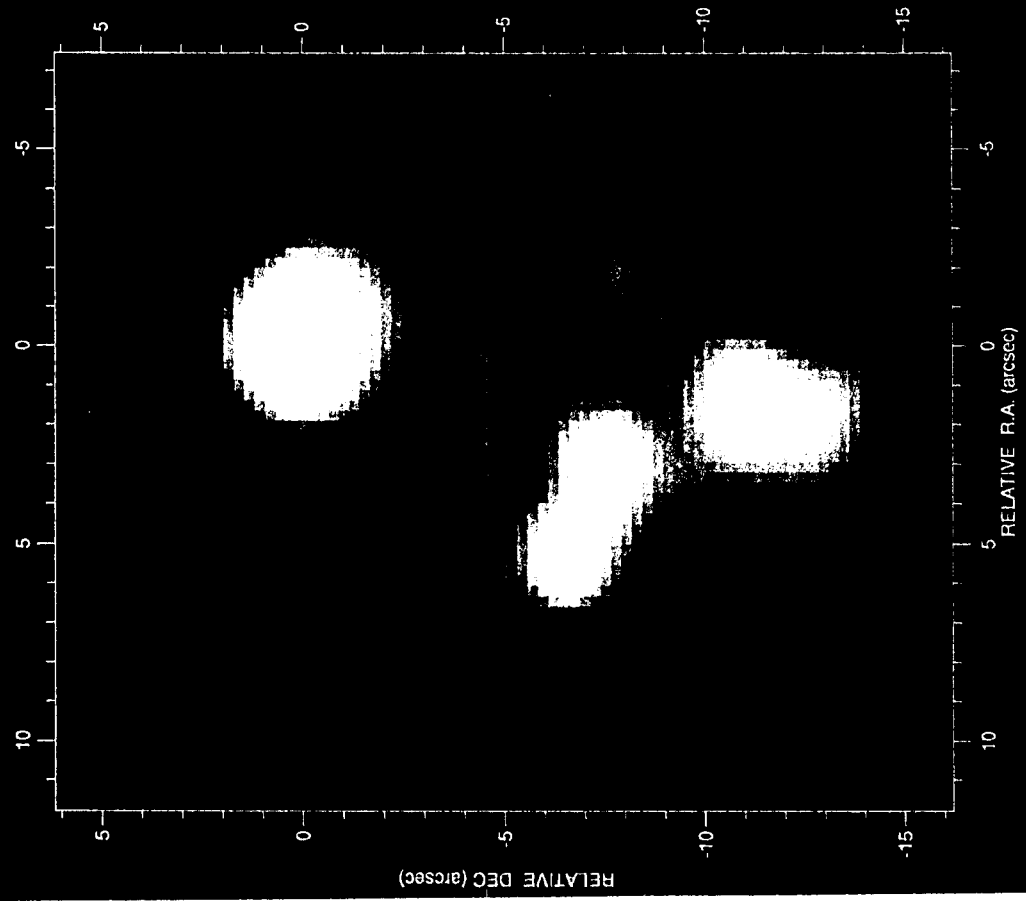


NASA/GSFC 5/29/97 D. Gezari

Fig. 3f

Orion\_upper\_folder/BN+KL-12.4.cal.mosaic  
Scaling, Linear (min= 0.0 max= 50.) Filter: smooth(3)

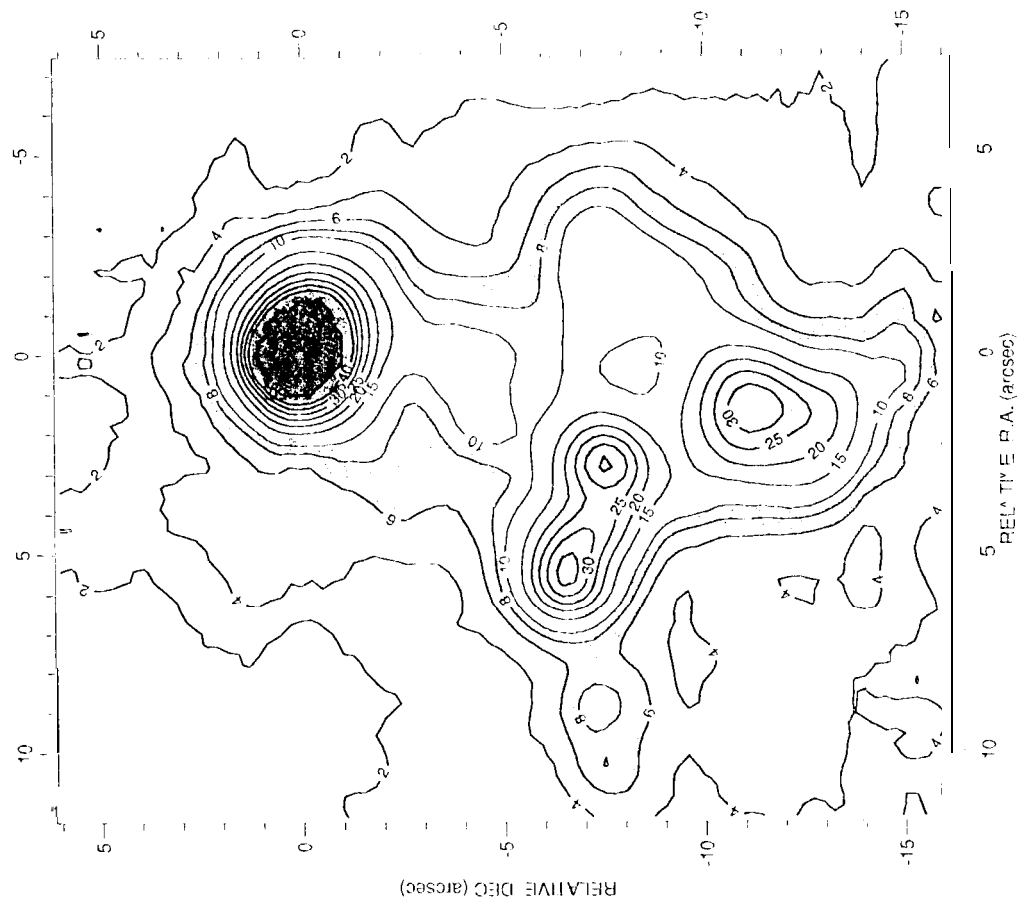
Orion BN/KL - 12.4  $\mu$ m



NASA/GSFC 5/29/97

Orion\_upper\_folder/BN+KL-12.4.cal.mosaic  
Contours, Linear (min=2.0 line=2.0 max=50. Fill: smooth(3)

Orion BN/KL - 12.4  $\mu$ m

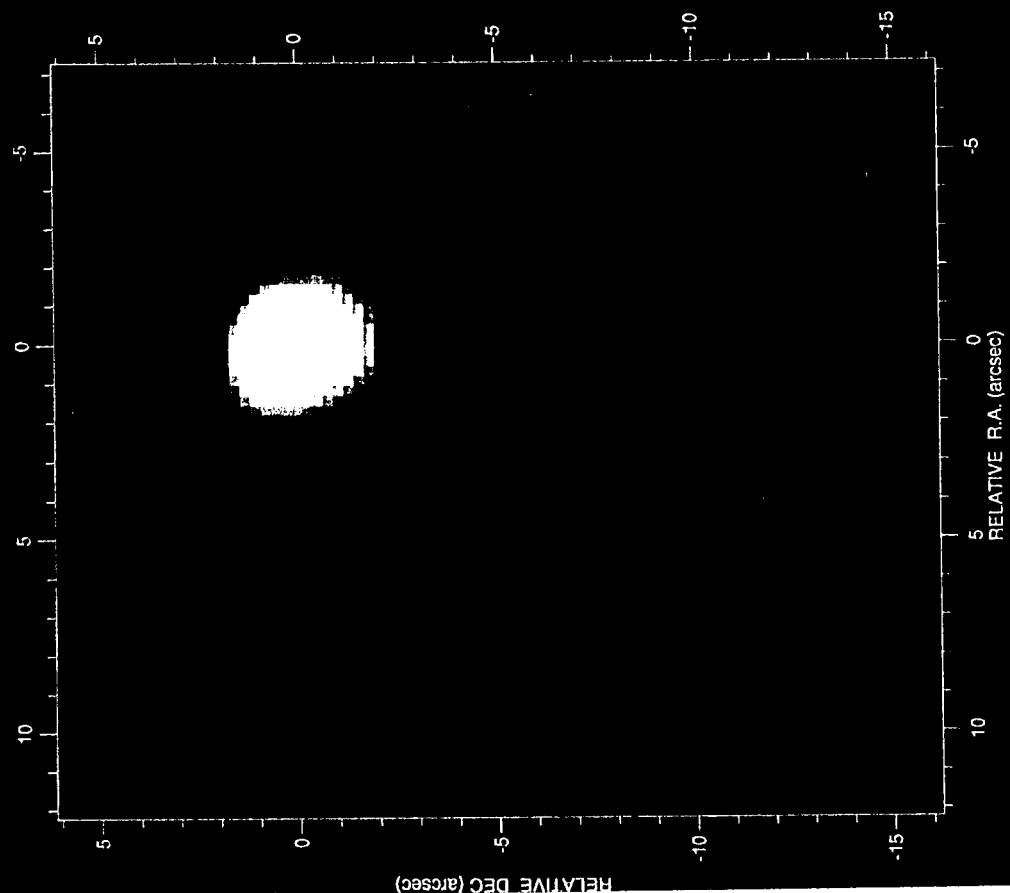


NASA/GSFC 5/29/97

Fig. 3a

Orion\_paper folder\BN/KL-18.1 umosaic  
Scaling: linear( min=-1.7E+03 max=1.2E+05) Filter: smooth(3)

Orion BN/KL - 18.1 um

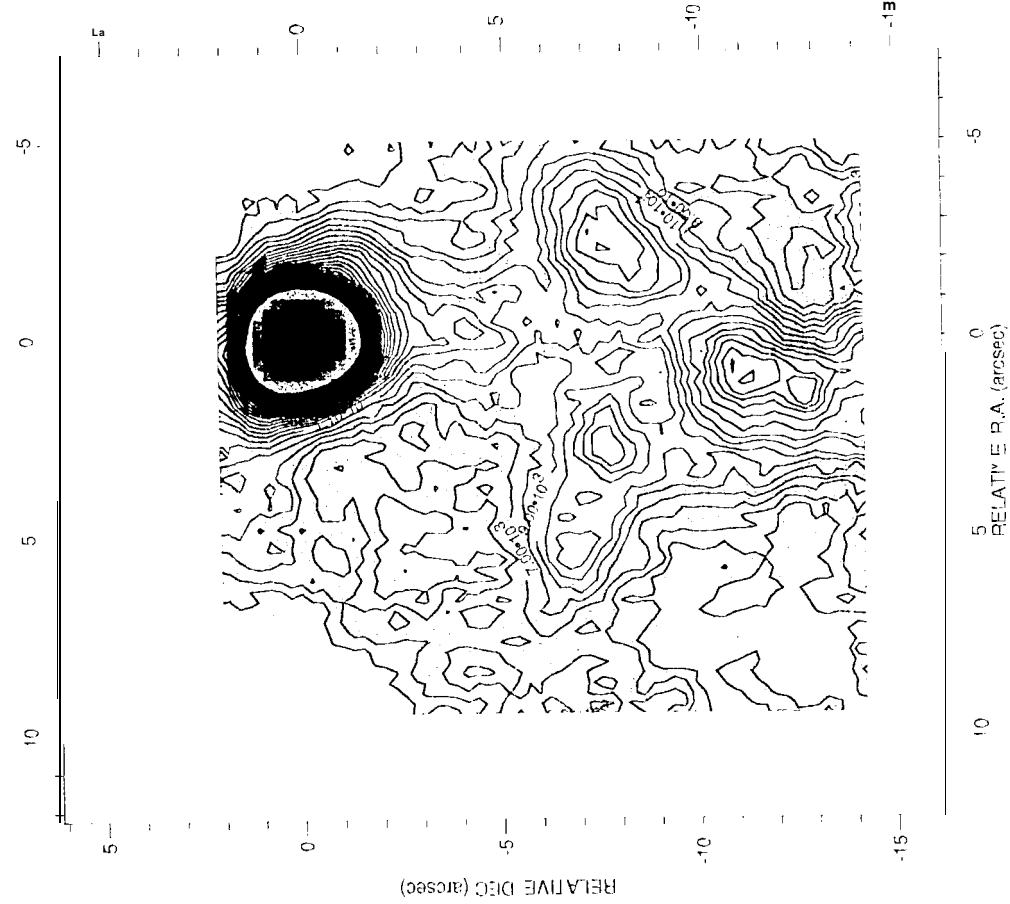


NASA/GSFC 5/29/97 D. Gezari

Fig 3h

Orion\_paper folder\BN/KL-8. umosaic  
Contour: Linear( min=5.0E+02 max=3.4E+04) Filter: smooth(3)

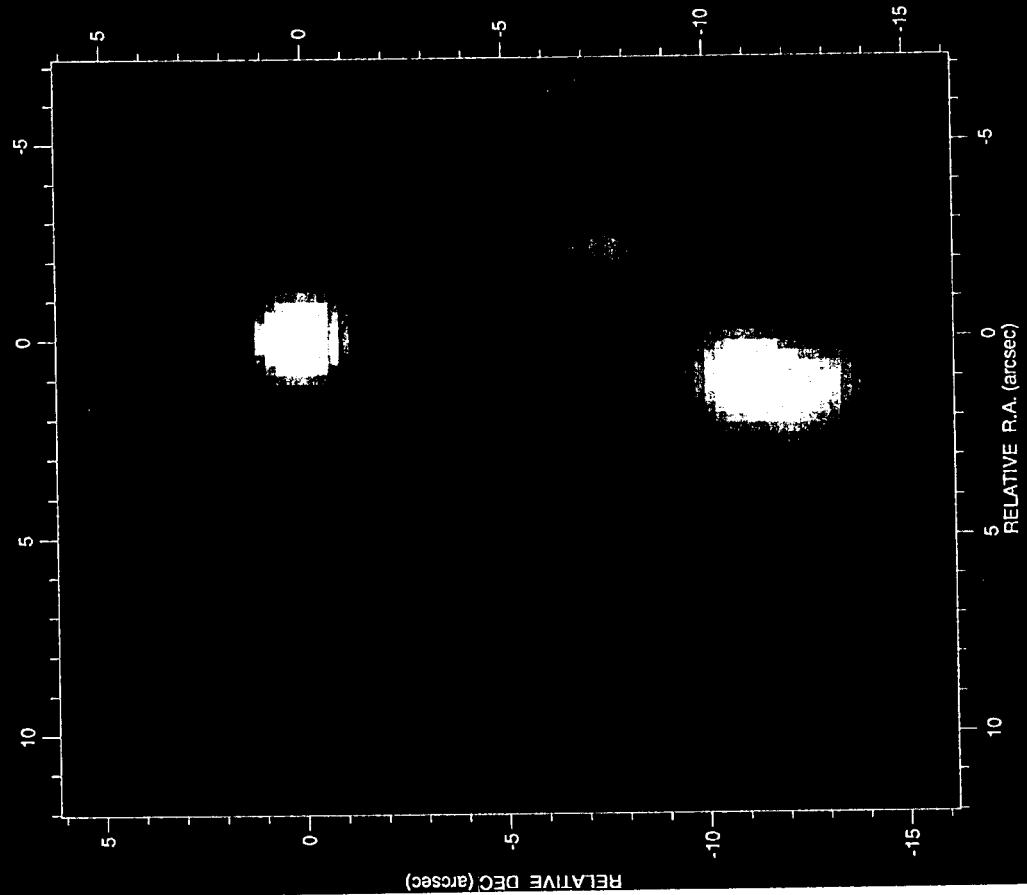
Orion BN/KL 8. um



NASA/GSFC 5/29/97 D. Gezari

Orion\_baper\folder\BN+KL-20.0.cal.mosaic  
Scratch Linear (nlhs= -12, mxs= 1.9E+02) Filter: smooth(3)

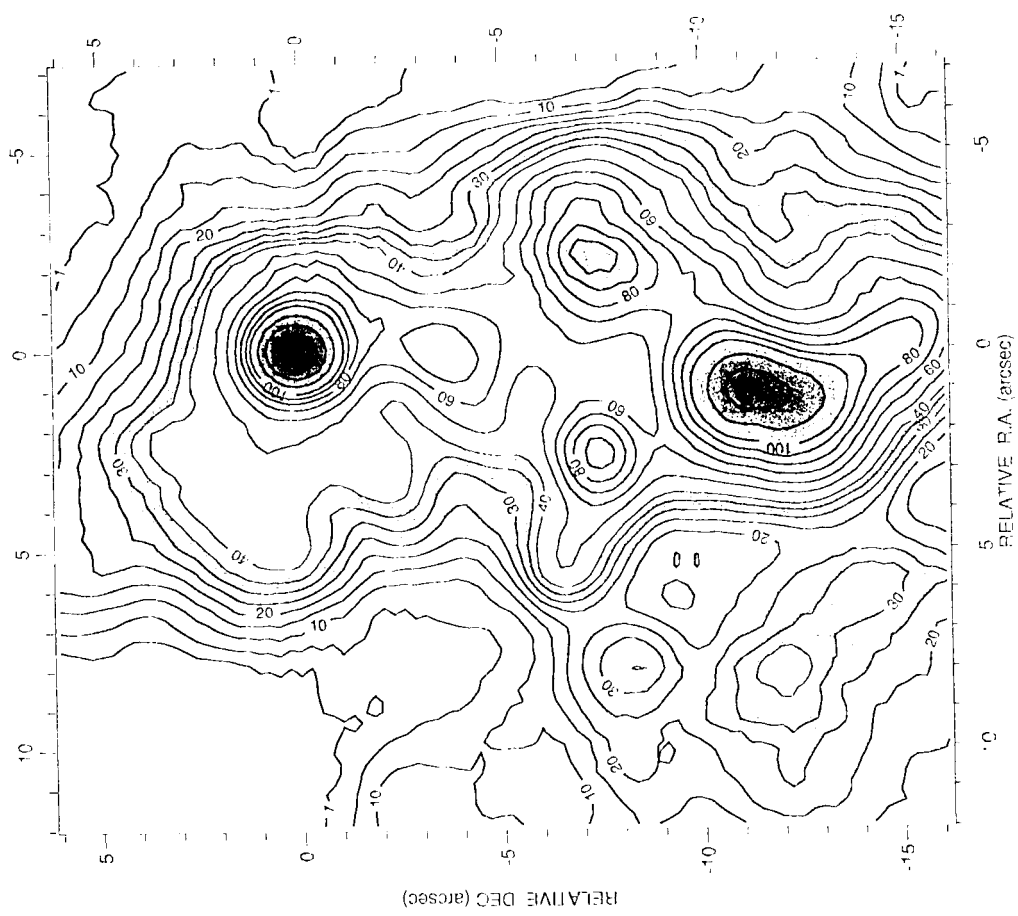
Orion BN/KL - 20.0 um



NASA/GSFC 5/29/97

Orion\_baper\folder\BN+KL-20.0.cal.mosaic  
Scratch Linear (nlhs= 1.0, mxs= 4.0, max= 1.9E+02) Filter: smooth(3)

BN/KL 20.0 um



NASA/GSFC 5/29/97

Fig. 30

### Orion BN/KL - Compact Infrared Sources

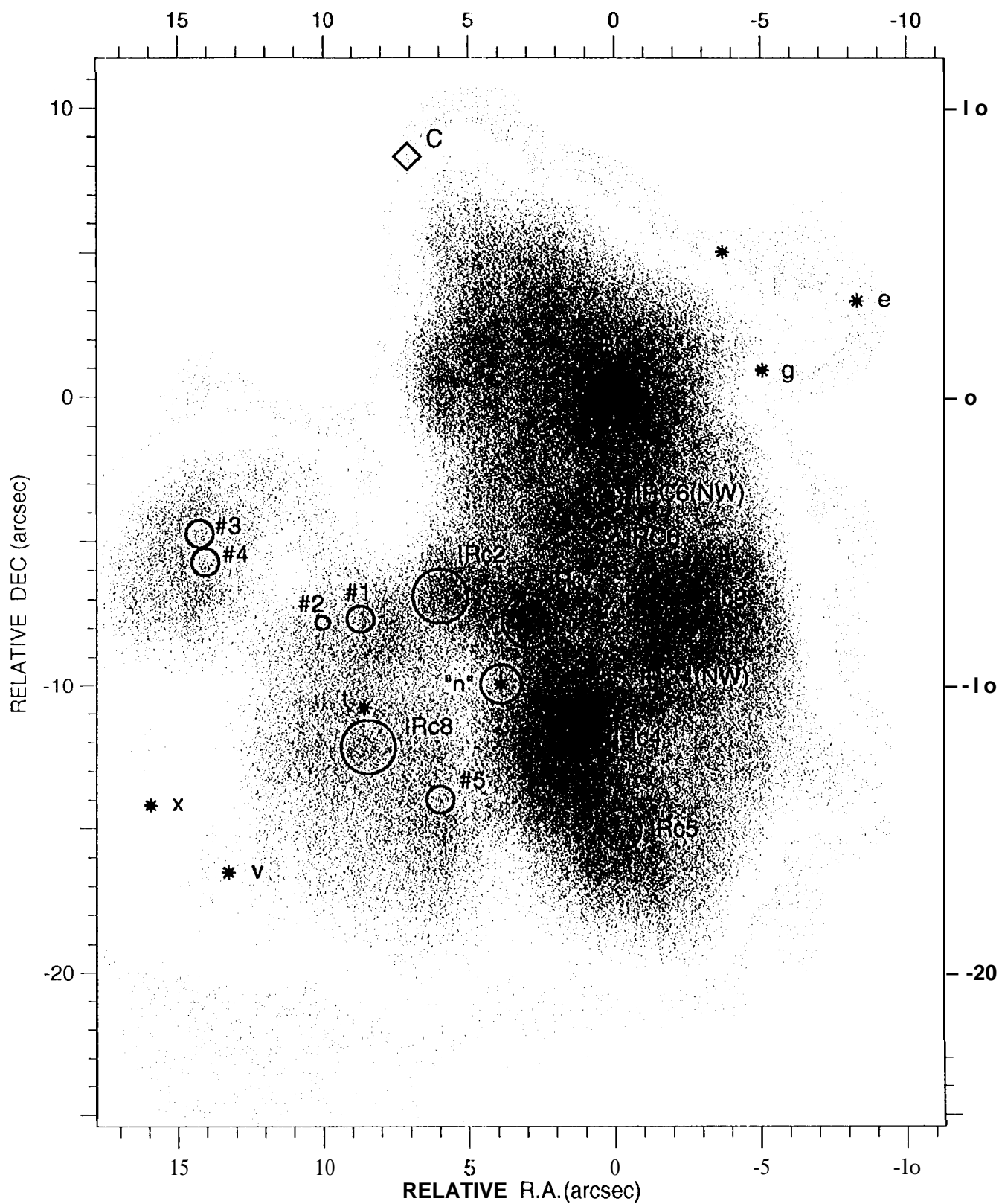


Figure 4

Orion BN/KL - 8.7 urn

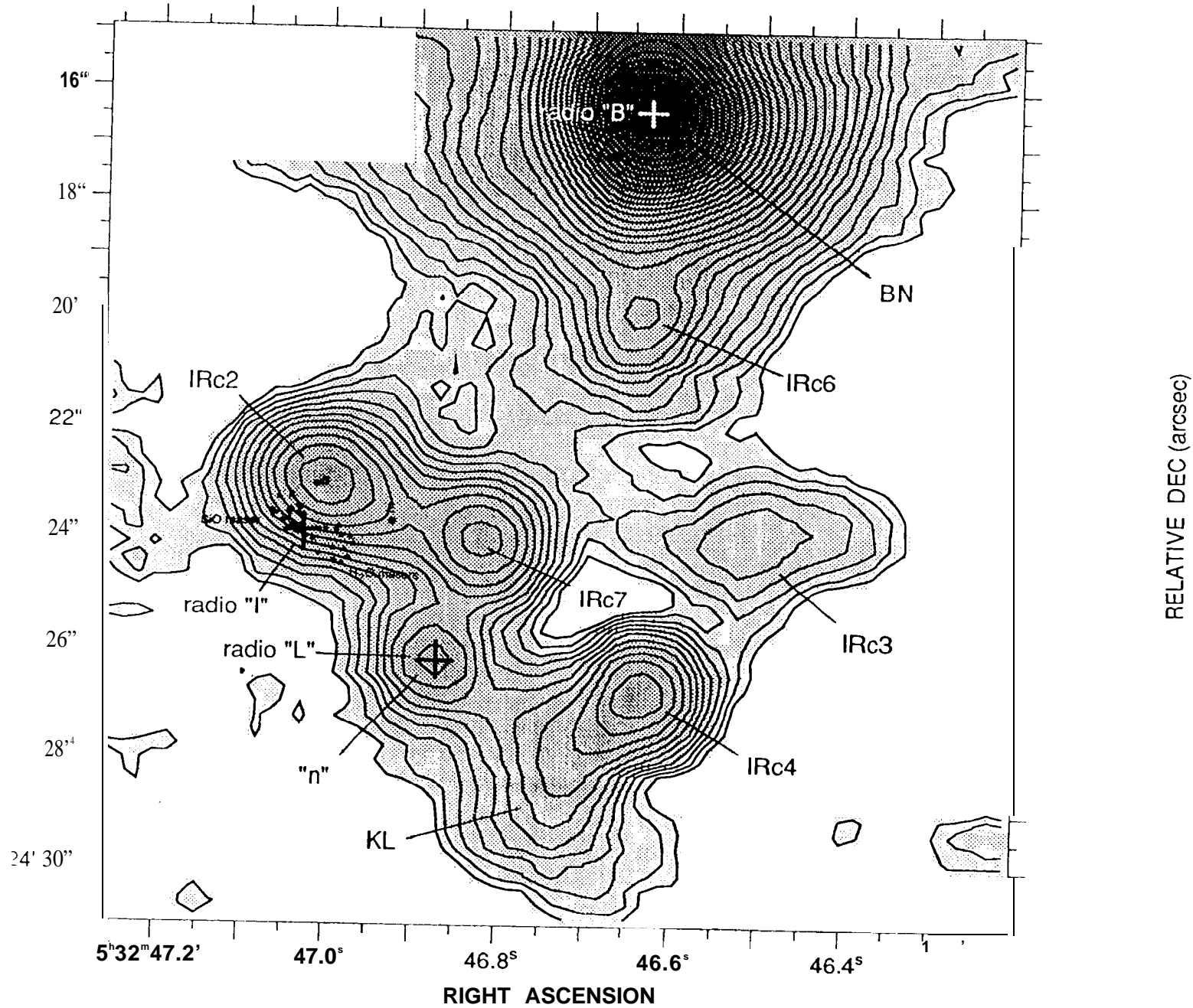


Fig. 5

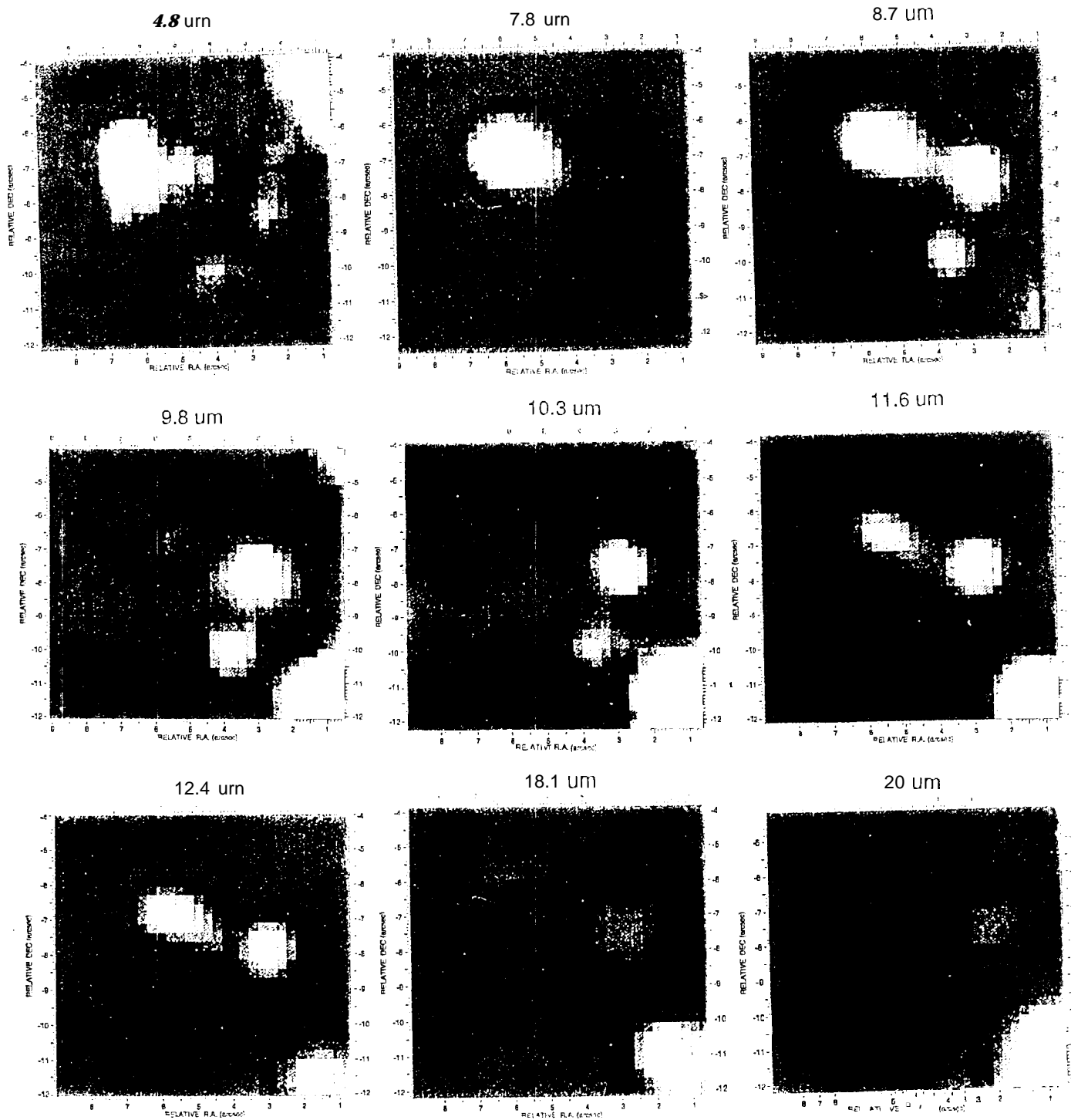


Figure 6

Silicate (9.8um) Extinction Factor

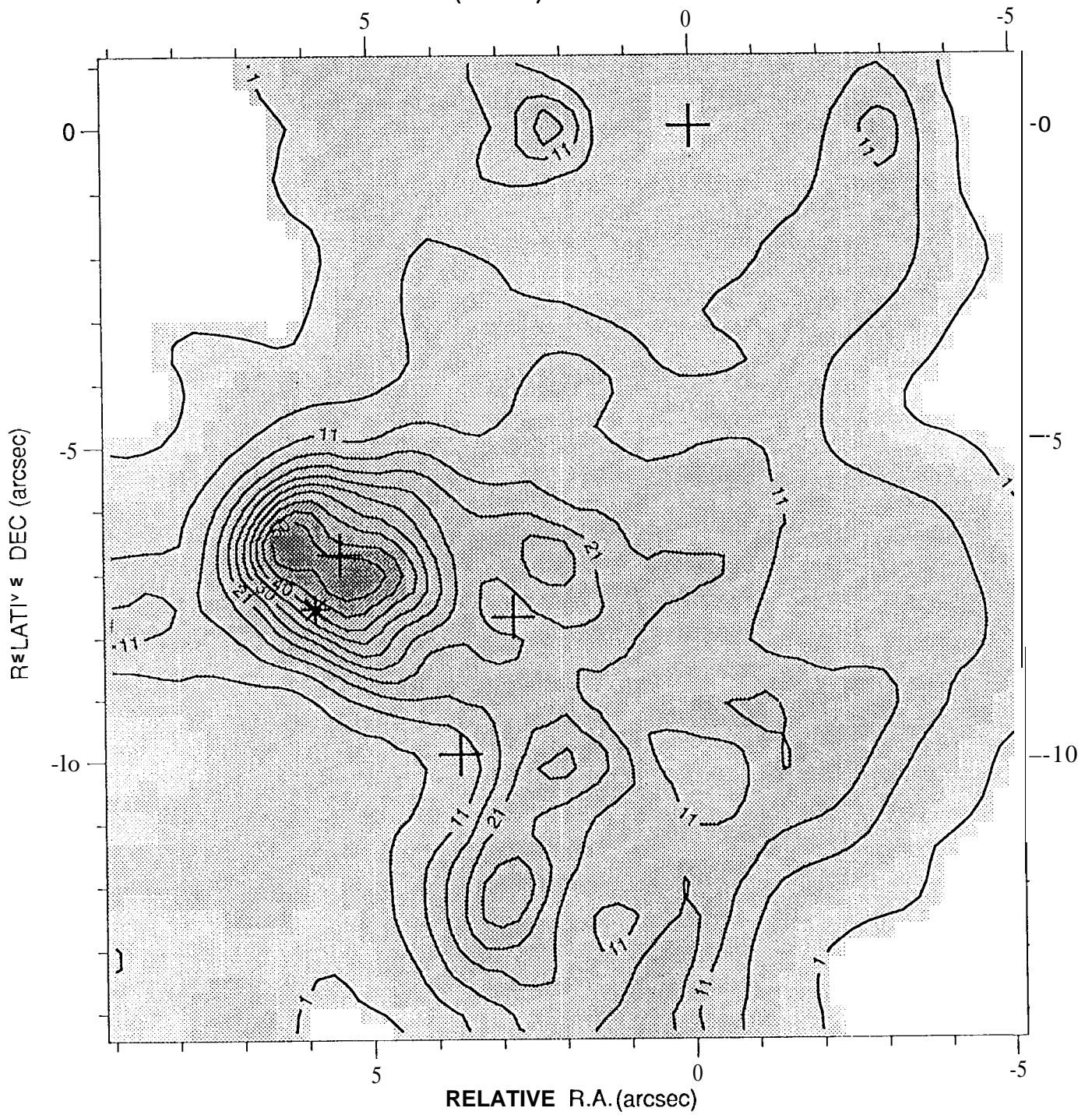


Figure 7

Ratio 20/12.4  $\mu\text{m}$  - Orion BN/KL

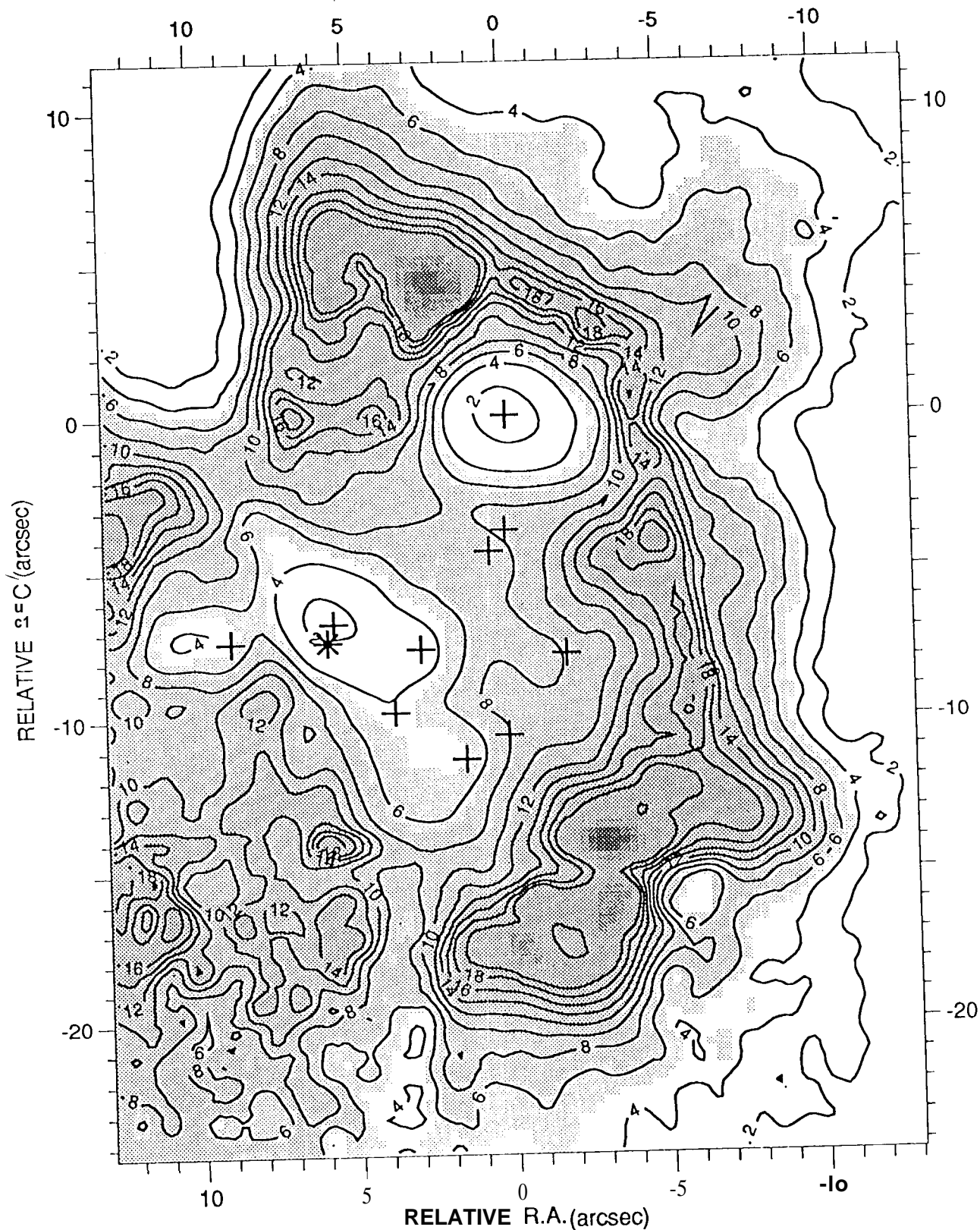


Figure 8

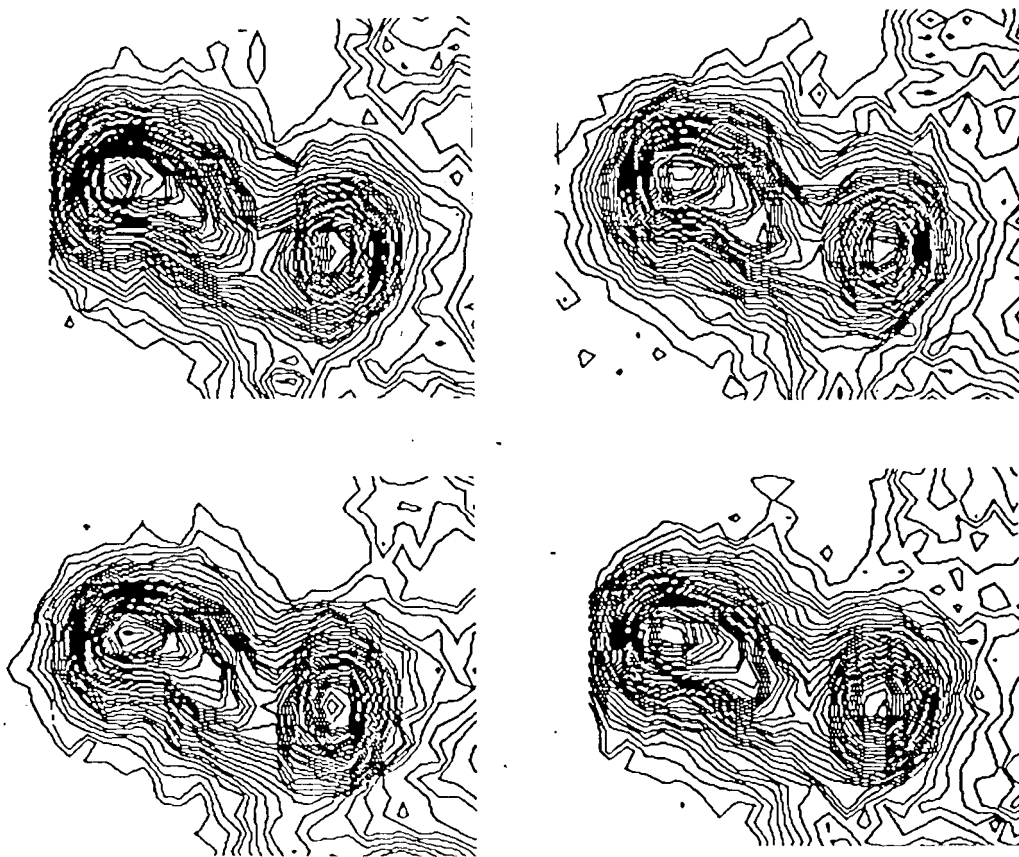


Figure 9

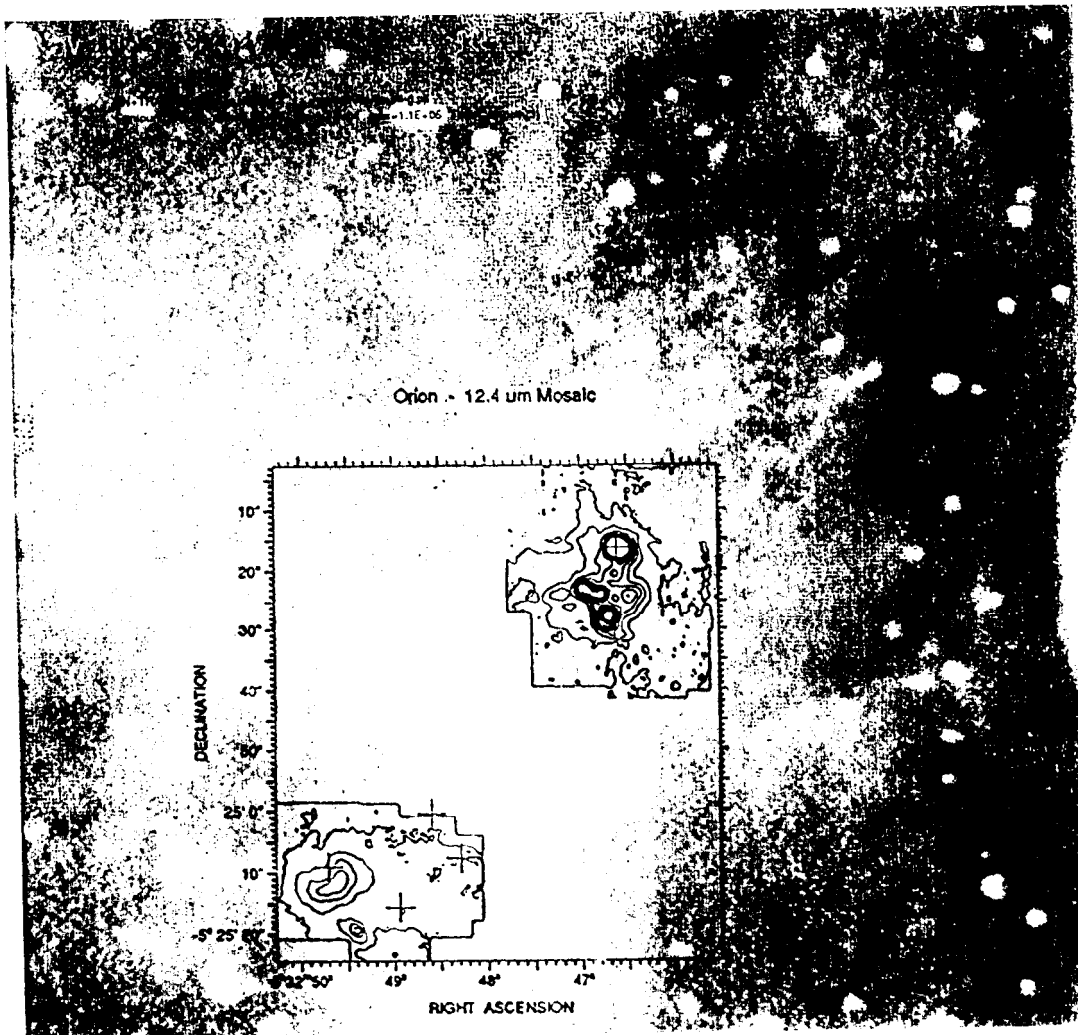


Fig. 10